Article:

Koenig, T. K., Volkamer, R., Baidar, S. et al. (39 more authors) (2017) BrO and Bry profiles over the Western Pacific:Relevance of Inorganic Bromine Sources and a Bry Minimum in the Aged Tropical Tropopause Layer. Atmospheric Chemistry and Physics Discussions. pp. 1-46. ISSN: 1680-7367

https://doi.org/10.5194/acp-2017-572

Atmos. Chem. Phys. Discuss., https://doi.org/10.5194/acp-2017-572
Manuscript under review for journal Atmos. Chem. Phys.
Discussion started: 7 July 2017

Atmospheric Chemistry and Physics
Discussions

BrO and Br_y profiles over the Western Pacific: Relevance of Inorganic Bromine Sources and a Br_y Minimum in the Aged Tropical Tropopause Layer

Theodore K. Koenig[1,2], Rainer Volkamer[1,2], Sunil Baidar[1,2,#], Barbara Dix[1], Siyuan Wang[2,3], Daniel C. Anderson[4,†], Ross J. Salawitch[4,5,6], Pamela A. Wales[5], Carlos A. Cuevas[7], Rafael P. Fernandez[7,8], Alfonso Saiz-Lopez[7], Mathew J. Evans[9], Tomás Sherwen[9], Daniel J. Jacob[10,11], Johan Schmidt[12], Douglas Kinnison[13], Jean-François Lamarque[13], Eric C. Apel[13], James C. Bresch[13], Teresa Campos[13], Frank M. Flocke[13], Samuel R. Hall[13], Shawn B. Honomichl[13], Rebecca Hornbrook[13], Jørgen B. Jensen[13], , Richard Lueb[13], Denise D. Montzka[13], Laura L. Pan[13], J. Michael Reeves[13], Sue M. Schauffler[13], Kirk Ullmann[13], Andrew J. Weinheimer[13], Elliot L. Atlas[14], Valeria Donets[14], Maria A. Navarro[14], Daniel Riemer[14], Nicola J. Blake[15], Dexien Chen[16], L. Gregory Huey[16], David J. Tanner[16], Thomas F. Hanisco[17], Glenn M. Wolfe[17,18]

[1]Department of Chemistry & Biochemistry, University of Colorado, Boulder, CO, USA
[2]Cooperative Institute for Research in Environmental Sciences (CIRES), Boulder, CO, USA
[3]Department of Chemistry, University of Michigan, Ann Arbor, MI, USA
[4]Department of Atmospheric & Oceanic Science, University of Maryland, College Park, MD, USA
[5]Department of Chemistry & Biochemistry, University of Maryland, College Park, MD, USA
[6]Earth System Science Interdisciplinary Center, University of Maryland, College Park, MD, USA
[7]Department of Atmospheric Chemistry and Climate, Institute of Physical Chemistry Rocasolano, Spanish National Research Council (CSIC), Madrid, Spain
[8]Argentine National Research Council (CONICET), FCEN-UNCuyo, UNT-FRM, Mendoza, Argentina
[9]Wolfson Atmospheric Chemistry Laboratories (WACL), Department of Chemistry, University of York, York, United Kingdom
[10]John A. Paulson School of Engineering and Applied Sciences, Harvard University, Cambridge, MA, USA
[11]Department of Earth and Planetary Sciences, Harvard University, Cambridge, MA, USA
[12]Department of Chemistry, Copenhagen University, Copenhagen, Denmark
[13]National Center for Atmospheric Research (NCAR), Boulder, CO, USA
[14] Department of Atmospheric Science, Rosenstiel School of Marine & Atmospheric Sciences (RSMAS), University of Miami, Miami, FL, USA
[15]Department of Chemistry, University of California, Irvine, CA, USA
[16]School of Earth & Atmospheric Sciences, Georgia Tech, Atlanta, Georgia, USA
[17]Atmospheric Chemistry and Dynamics Laboratory, NASA Goddard Space Flight Center, Greenbelt, Maryland, USA
[18]Joint Center for Earth Systems Technology, University of Maryland, Baltimore County, Maryland, USA
[#]now at: National Oceanic and Atmospheric Administration (NOAA), Boulder, CO, USA
[†]now at: Department of Chemistry, University of Drexel, Philadelphia, PA, USA

Correspondence to: Rainer Volkamer (rainer.volkamer@colorado.edu)

Abstract. We report measurements of bromine monoxide (BrO) and use an observationally constrained chemical box-model to infer total gas phase inorganic bromine (Br_y) over the tropical Western Pacific Ocean (tWPO) during the CONTRAST field campaign (January – February 2014). The median tropospheric BrO Vertical Column Density (VCD) over the tWPO was measured as 1.6×10^{13} molec. cm^{-2}, compared to model predictions of 0.4×10^{13} in CAM-Chem, 0.9×10^{13} in GEOS-Chem, and 2.1×10^{13} in GEOS-Chem with a sea-salt aerosol (SSA) bromine source. The observed BrO and inferred Br_y profiles is found to be C-shaped in the troposphere, with local maxima in the marine boundary layer (MBL) and in the upper free troposphere. Neither global model fully captures this profile shape. Between 6 and 13.5 km, the inferred Br_y is highly sensitive to assumptions about the rate of heterogeneous bromine recycling (depends on the surface area of ice/aerosols), and the inclusion of a SSA bromine source. A local Br_y maximum of 3.6 ppt (2.3-11.1 ppt, 95% CI) is observed between 9.5 and 13.5 km in air masses influenced by recent convective outflow. Unlike BrO, which increases from the convective TTL to the aged TTL, gas phase Br_y decreases from the convective TTL to the aged TTL. Analysis of gas phase Br_y against multiple tracers (CFC-11, H_2O/O_3 ratio, and θ) reveals a Br_y minimum of 2.7 ppt (2.4-3.0 ppt, 95% CI) in the aged TTL, which is remarkably insensitive to assumptions about heterogeneous chemistry. Br_y increases to 6.3 ppt (5.9-6.7 ppt, 95% CI) in the stratospheric middleworld, and 6.9 ppt (6.7-7.1 ppt, 95% CI) in the stratospheric overworld. The local Br_y minimum in the aged TTL is qualitatively (but not quantitatively) captured by CAM-chem, and suggests a more complex partitioning of gas phase and aerosol Br_y species than previously recognized. Our data provide corroborating evidence that inorganic bromine sources (e.g., SSA derived gas phase Br_y) are needed to explain the gas phase Br_y budget in the TTL. They are also consistent with observations of significant bromide in UTLS aerosols. The total Br_y budget in the TTL is currently not closed, because of the lack of concurrent quantitative measurements of gas phase Br_y species (i.e., BrO, HOBr, HBr, etc.) and aerosol bromide. These simultaneous measurements are needed 1) to quantify SSA derived Br_y aloft, 2) to test Br_y partitioning, and explain the gas phase Br_y minimum in the aged TTL, 3) to constrain heterogeneous reaction rates of bromine, and 4) to account for all of the sources of Br_y to the lower stratosphere.

1 Introduction

Gas phase bromine in the atmosphere can be divided into organic and inorganic species. Inorganic bromine in the gas phase (Br_y) can be further divided into active bromine ($BrO_x = Br + BrO$), reservoir species (HBr, HOBr, $BrNO_2$, and $BrONO_2$), and photolabile compounds (Br_2 and BrCl). Atomic bromine (Br) and bromine monoxide (BrO) rapidly interconvert, primarily by reaction with O_3 and photolysis.

Reactions of BrO_x have a number of important impacts in the troposphere. First, BrO_x participates in catalytic reaction cycles that destroy ozone (von Glasow et al., 2004; Read et al., 2008; Saiz-Lopez and von Glasow, 2012; Schmidt et al., 2016; Simpson et al., 2015; Wofsy et al., 1975). Recent simultaneous measurements of BrO and IO over the tropical Eastern Pacific Ocean (tEPO) (Volkamer et al., 2015) suggest that, in the troposphere, bromine and iodine together account for 34% of column integrated ozone loss (Wang et al., 2015) and the global mean impact of all halogens reduces the ozone burden between 10 and 18% (Saiz-Lopez et al., 2012, 2014, Sherwen et al., 2016, 2017b). Second, BrO_x modifies NO_x ($= NO + NO_2$) by increasing the ratio of NO_2/NO (Bloss et al., 2010), and is an overall sink of NO_x (Schmidt et al., 2016), among other chemical effects (Custard et al., 2015; Evans et al., 2003; Lary, 2005). Third, BrO_x adds to oxidative capacity and exerts a number of competing effects on HO_x (= OH + HO_2). In particular, the lower ozone leads to a lower production of OH radicals from ozone photolysis; lower NO_x leads to a decrease in the OH/HO_2 ratio, and HOBr photolysis increases the OH/HO_2 ratio. A lower bound on the overall impact is an 11% reduction in OH (Schmidt et al., 2016), subject to uncertainty in the representation of heterogeneous bromine recycling and sea-salt sources. Fourth, BrO_x is thought to be the primary oxidant of mercury in the atmosphere (Coburn et al., 2016; Goodsite et al., 2004; Holmes et al., 2006) and an important loss mechanism for dimethyl sulfide (Boucher et al., 2003). Fifth, the net-effect of BrO_x impacts on O_3, NO_x, and HO_x leads to an increase of the lifetime of CO and hydrocarbons (Lelieveld et al., 1998; Parrella et al., 2012; Saiz-Lopez and von Glasow, 2012). The combined impact of halogen destruction of OH on the lifetime of methane has most recently been found to be an increase of 6.5% (Sherwen et al., 2016).

Bromine also has important impacts in the stratosphere, where the ozone destruction potential is ~60 times higher than that of chlorine (on a per atom basis) (Sinnhuber et al., 2009). Historically, the source of stratospheric bromine has been thought to be analogous to chlorine, resulting from the source gas injection (SGI) of longer lived organic bromine species (LLS) — of both anthropogenic natural origin — into the stratosphere. However, measurements of stratospheric Br_y generally exceed the abundance of Br_y that can be explained from SGI of LLS alone (Carpenter and Reimann et al., 2014; Salawitch et al., 2005). Very Short Lived Species (VSLS, i.e., bromoform ($CHBr_3$), dibromomethane (CH_2Br_2)) directly add to SGI, and their photolysis and oxidation in the troposphere adds inorganic bromine as Product Gas Injection (PGI) into the LS (Ko and Poulet et al., 2003). Recent measurements of elevated BrO in the free troposphere (FT) suggest sea-salt sources may contribute to Br_y in the FT (Volkamer et al., 2015; Wang et al., 2015; Schmidt et al., 2016), but the relative contribution of sea-salt derived Br_y and VSLS derived PGI contributions to stratospheric Br_y injection has to our knowledge not previously been experimentally evaluated. One objective of the CONvective TRansport of Active Species in the Tropics (CONTRAST) and the Airborne Tropical TRopopause EXperiment (ATTREX) field campaigns (January and February 2014) in Guam was to provide observational constraints to Br_y from aircraft measurements of BrO in the upper troposphere - lower stratosphere (UTLS) over the tropical Western Pacific Ocean (tWPO) (Chen et al., 2016; Jensen et al., 2016; Pan et al., 2017; Werner et al., 2017).

Differential optical absorption spectroscopy (DOAS) measurements of BrO have been made in the tropics from satellites (Chance, 1998; Richter et al., 2002; Theys et al., 2011; Wagner et al., 2001), ground-based Multi AXis –DOAS (MAX-DOAS) (Theys et al., 2007), balloon profiles (Dorf et al., 2006, 2008; Pundt et al., 2002), and airborne platforms (Volkamer et al., 2015; Wang et al., 2015; Werner et al., 2017). In addition to DOAS, microwave emission techniques have also been employed to measure BrO (Millán et al., 2012; Stachnik et al., 2013). Chemical Ionization Mass Spectrometry (CIMS) measurements of atmospheric Br_y, using I^- or SF_6^-, have largely been limited to BrO, although BrCl, HOBr, and Br_2 have also been detected (Le Breton et al., 2017; Chen et al., 2016; Neuman et al., 2010).

Here we describe measurements of BrO by the University of Colorado Airborne MAX-DOAS instrument aboard the NCAR/NSF Gulfstream V (GV) aircraft during CONTRAST field campaign (January and February 2014) in Guam. The GV carried a suite of in-situ and remote sensing instruments designed to characterize atmospheric composition targeting bromine species, including bromocarbons and inorganic bromine species, as well as dynamical properties. An overview of the campaign is available in (Pan et al., 2017). The campaign consisted of 17 research flights (RFs). Numerous flights were in/near clouds, and presented challenges for DOAS retrievals. We focus the analysis on portions of five flights: RF03, RF04, RF06, RF07, and RF15, which were conducted in largely cloud free air. RF03, RF04 and RF07 were chosen for vertical profiles over the tWPO, covering altitudes from the boundary layer up to the lower tropical tropopause transition layer (TTL) on 19, 21, and 27 January 2014. The flight paths of RF06 and RF15 were to the north of Guam and targeted the northern hemisphere extratropical jet stream on 25 January and 25 February of 2014 respectively. For RF15, the GV crossed the jet-stream and sampled the the northern hemisphere lower stratosphere.

2 Experimental

The University of Colorado Airborne Multi AXis Differential Optical Absorption Spectroscopy (CU AMAX-DOAS) aboard the GV measured trace gases including the halogen oxides BrO and IO, and NO_2. Additional species such as formaldehyde (HCHO), O_3, H_2O and glyoxal can also be retrieved. Other instruments and measurements aboard the GV included but were not limited to: the Advanced Whole Air Sampler (AWAS), which measured species including halocarbons and a variety of chemical tracers; the HIAPER Atmospheric Radiation Package (HARP), which measured actinic flux and photochemical rates; the Trace Organic Gas Analyzer (TOGA), which measured organic species including halocarbons and aldehydes; chemiluminescent measurements of NO, NO_2 and O_3; Picarro CRDS instruments which measured CO_2 and CH_4; a Vacuum Ultra Violet fluorescence instrument (Aerolaser) which measured CO; the In Situ Airborne Formaldehyde (ISAF) instrument whcih measured HCHO; and, the Ultra-High Sensitivity Aerosol Spectrometer (UHSAS) which measured size resolved Aitken and accumulation mode aerosol. The measurements used in this work are summarized in Table 1.

2.1 CU AMAX-DOAS instrument

The University of Colorado Airborne Multi AXis Differential Optical Absorption Spectroscopy (CU AMAX-DOAS) instrument has been deployed during field campaigns in urban air (Baidar et al., 2013; Oetjen et al., 2013), and over remote oceans (Dix et al., 2013; Volkamer et al., 2015), and is described in detail in these papers. Briefly, the CU AMAX-DOAS consists of a wing-mounted pylon containing a motion stabilized telescope, and two spectrographs housed in the interior of the aircraft. Scattered sunlight enters the telescope along a well-defined field of view (vertical dispersion of 0.17°) and is actively motion stabilized with a pointing accuracy better than 0.2° in real time (Baidar et al., 2013; Volkamer et al., 2015). Elevation angles (EA) above geopotential horizontal are positive, those below are negative, zero EA points forward of the aircraft. Viewing windows provide an unobstructed view to shallow angles (-30° to +30°) as well as zenith and nadir geometries. Light entering the telescope travels through fiber optic bundles to two spectrograph-detector units, each consisting of an Acton SP2150 spectrograph coupled to a PIXIS400B CCD. The units are operated synchronously, integrating spectra every 30 s. One Acton SP2150/PIXIS400B CCD unit (AP1) covers the spectral range from 330-470 nm with 0.7 nm full width half maximum (FWHM) optical resolution. The other (AP2) measures 440-700 nm at 1.2 nm FWHM resolution. Spectra collected on AP1 are used for the measurement of BrO, glyoxal, HCHO, H_2O, IO, NO_2 (360 nm and 450 nm), and O_4 (360 nm); spectra on AP2 are used for the measurement of NO_2 (560 nm) and O_4 (477 nm). In this work only BrO, NO_2 (360 nm), and O_4 (360 nm) results will be presented, using EA 0° spectra collected with 30 s integration times. Zenith spectra with at least two minute integration times collected at low altitude under relatively clear skies were used as reference spectra. Low altitude zenith spectra were used as references, with the nearest qualifying spectrum in time being used. In all instances the reference was from the same RF. The specific settings used are discussed in Section 2.1.1.

Differential Slant Column Densities (dSCDs) of BrO are the primary data product from the AMAX-DOAS. O_4 dSCDs are used to constrain atmospheric radiative transfer in one of two ways optimal estimation to obtain explicit aerosol extinction profiles, or parameterized using a ratio of measured O_4 dSCDs with those modeled in a Rayleigh atmosphere. Combination of this radiative information with the BrO dSCDs is used to obtain BrO mixing ratios as vertically resolved profiles (Volkamer et al., 2015) through optimal estimation and along the flight track by a parameterization method (Dix et al., 2016). These processes are outlined in greater detail in Section 2.1.2.

When using parameterization data in the box model, we account for the fact that the AMAX-DOAS instrument detects photons scattered at a variety of distances along the line of sight. The median photon is scattered 5 - 70 km forward of the plane, depending on altitude and aerosol conditions. This difference between air masses sampled by AMAX-DOAS and the in-situ observations was accounted for as follows: when the aircraft maintains its heading, AMAX-DOAS data are taken to correspond to the air mass where the median photon was scattered, which is then sampled by in situ instruments with some delay (typically 4.5-6.0 min). The atmosphere used for radiative transfer modeling accounts for this delay using model information from the same location. When the aircraft changes heading, the AMAX-DOAS data are matched to the in-situ data nearest in altitude and latitude.

2.1.1 DOAS retrieval

Trace gases were fit using the DOAS method (Platt and Stutz, 2008) using the QDOAS software package (Danckaert et al., 2012). The wavelength calibration for each spectrum is precisely determined by measuring the mercury atomic emission at 404.7 nm. This slit function was further refined by fitting two wavelength dependent degrees of freedom, using the Kurucz spectrum as reference. The slit function was fixed for final calibration of the instrument wavelength mapping. High resolution laboratory cross-sections (species and references given in Table 2) are convolved with the instrument function for analysis. Broadband extinction including Mie and Rayleigh scattering is accounted for by a polynomial. Trace gases with broad band absorption components such as O_3 and NO_2 are orthogonalized to this polynomial. A linear intensity offset is included in some settings to account for instrumental stray light and imperfect knowledge of the Ring effect (Grainger and Ring, 1962). Absorption by relevant species is fitted simultaneously by a non-linear least squares fitting routine in finite wavelength windows targeting specific trace gases. The analysis settings for BrO, NO_2, and O_4 (360 nm) are summarized in Table 2.

BrO was analyzed using a four-band analysis in the window 335 nm – 359 nm. The broader window was chosen to maximize information on other absorbers. The overlapping O_4 was accounted for by first determining accurate O_4 dSCDs using an optimized fit window, and prescribing these O_4 dSCDs in the BrO fit. Information on O_4 in the BrO fitting window is maximized at wavelengths of greatest differential absorption by this dimer, namely at the peak at 343 nm and the shoulder at the window edge at 359 nm. The O_4 cross-section has been scaled to reflect the shorter path length of photons through the atmosphere at the lower wavelengths, using a λ^{-4} dependence, which is based on the assumption that Rayleigh scattering dominates. The mixing ratio of NO_2 was retrieved for the RF15 case study, and used to constrain the box model (Supplement, Fig. S1).

2.1.2 Radiative Transfer Modeling

Simulations were run using the Monte Carlo radiative transfer model McArtim (Deutschmann et al., 2011) in a 1D spherical atmosphere. Aerosol extinction is accounted for by taking advantage of the fact that the atmospheric profile of [O_4] is highly predictable, namely it scales as the square of the [O_2], which has an essentially constant mixing ratio at altitudes of interest and scales linearly as a function of density (Spinei et al., 2015; Thalman and Volkamer, 2013). Comparison of modeled and measured O_4 SCDs is done in one of two ways: parameterization (Dix et al., 2016) of aerosol effects using a ratio, or retrieval of explicit aerosol profiles (Baidar et al., 2013; Volkamer et al., 2015). The high accuracy of the Rayleigh scattering cross-sections represented in the Radiative Transfer Model (RTM), and O_4 dSCD measurements used by the parameterization method has been independently evaluated by laboratory measurements (Thalman et al., 2014), field observations in the absence (Spinei et al., 2015) and in the presence of aerosols (Volkamer et al., 2015).

The parameterization method is discussed in detail in Dix et al. (2016). Briefly, the method makes use of the fact that spectra recorded with EA 0° are strongly sensitive to the atmospheric layer at instrument altitude. Recorded EA 0° spectra are analyzed using reference spectra that largely cancel out column contributions from above and below the instrument. The conversion of dSCDs into VMRs is realized by calculating box-AMFs for a Rayleigh atmosphere and applying a scaling factor constrained by O_4 dSCDs to account for aerosol extinction. The color ratio of the measured intensities at 477 nm and 640 nm is used to identify and filter measurements affected by clouds. Cloud filtering is manually quality controlled using aircraft video data and adapted where needed. An iterative VMR retrieval scheme corrects for trace gas profile shape effects. Profile information is gained from DOAS measurements during ascents and descents, and interpolated above the aircraft based on CAM-chem profiles. For stratospheric absorbers like BrO and NO_2, a stratospheric correction is included. The magnitude of the stratospheric correction is characterized by periodically upward looking EA 10° spectra and interpolated between successive EA 10° measurements, assuming profile shapes from CAM-chem. During portions of RF15 the telescope pointing exhibited a small positive bias of $< 1°$. This effect was well characterized at all times, and has been accounted for in the analysis. To account for horizontal concentration gradients, especially near the jet, photons are modelled in a horizontally homogenous atmosphere constructed using measurements and models for the zonal location of the median photon scattering. Errors are the total of the following three components added in quadrature: 1) a parameterization error of 30% but no better than 0.5 ppt; 2) the standard error of the mean of the component 30 s dSCDs; 3) the quadratic mean of the proportional dSCD errors of the component 30 s dSCDs.

For the optimal estimation method, aerosol profiles are retrieved by seeking to reproduce the measured O_4 SCDs. O_4 SCDs are primarily sensitive to aerosol extinction over other aerosol radiative properties, which are set to values expected to be typical of the local atmosphere. Settings are summarized in Table S1. Where O_4 dSCDs are lower than modeled, aerosol extinction is increased to achieve better agreement (Volkamer et al., 2015). An onion peeling approach is used to retrieve an initial aerosol profile, which is adjusted by hand until modeled and measured O_4 SCDs converge (Baidar et al., 2013). Extinction profiles retrieved at 200 m vertical resolution at 360 nm are presented in panels A of Fig. S2. Total aerosol optical depth was 0.304 in RF03, 0.272 in RF04, and 0.231 in RF07. Agreement between measured and modelled O_4 is better than 2×10^{42} molec^2 cm^{-5} (8×10^{-4} optical density) and often better than 1×10^{42} molec^2 cm^{-5} (4×10^{-4} optical density) as shown in panels B of Fig. S2. An Ångström exponent (α) of 1 is assumed in adjusting the aerosol extinction from the 360 nm derived using O_4 to 350 nm relevant for BrO. Air mass factors for each measurement were modeled at 500 m resolution, the grid resolution used for BrO profile retrieval. The a priori profile was a constant mixing ratio of 0.05 ppt BrO (though retrievals were all found to be insensitive to the choice of the a priori profile). The a priori error was set to be 2,000% for RF03 and 10,000% for RF04 and RF07. The lower error for RF03 was chosen to increase the stability of the profile retrieval from 0.5-2.0 km, because the presence of a small cloud interfered with some spectra which have been excluded from the inversion. dSCD errors are propagated into the diagonal terms of the error covariance matrix. The error covariance matrix was constructed with an effective height of 0.5 km, resulting in nearest neighbor off-diagonal terms. The resulting averaging kernels for the inversion are shown in panels D of Fig. S2. For RF04 and RF07 they typically peak sharply near 1, indicating independent information for all layers. The effects of lower a priori error and removal of data collected in the presence of clouds are apparent in the averaging kernel profile for RF03, which has a gap near the surface. The mean averaging kernel peak values are 0.728, 0.953, and 0.962 for RF03, RF04 and RF07, respectively. The total degrees of freedom are 18.2, 17.2 and 26.9 for RF03, RF04, and RF07 profiles, respectively.

2.2 Other Measurements

A number of other instruments were aboard the NCAR GV during the CONTRAST field campaign (Pan et al., 2017). Data used to constrain the box model are summarized in Table 1. More detailed descriptions of the instruments can be found in the supplement.

2.3 Model Descriptions

Data from the AMAX-DOAS and other instruments were combined and used to initialize a box model (Wang et al., 2015) in order to examine partitioning of inorganic bromine (Br_y), specifically the ratio BrO/Br_y, and infer gas phase Br_y from the BrO measurements. In addition BrO, Br_y, and Br_y speciation were also obtained from two Chemical Transport Models (CTM): the Goddard Earth Observing System with Chemistry model (GEOS-Chem) (Schmidt et al., 2016; Sherwen et al., 2016) and the Community Atmospheric Model with Chemistry model (CAM-Chem) (Fernandez et al., 2014) for purposes of comparison.

2.3.1 Box Model

The box model has been previously described in Wang et al. (2015). The model calculates gas phase Br_y bromine partitioning, and is constrained to measurements of chemical species and meteorological parameters as summarized in Table 1, and Sect. 2.2. The model was initialized every 5 min along the flight track. In general, data collected at a time resolution of ~30 s or at higher frequency were averaged into 5 min bins, and used as inputs to the box model; lower frequency data were linearly interpolated. For profile case studies horizontal homogeneity was assumed and in situ and remote sensing data were matched by altitude. For horizontal case studies, the AMAX-DOAS data were matched with in situ data sampled from the location of the median photon, as elaborated below. Sensitivity studies were conducted to bound the impacts of uncertainties in chemical kinetics and available surface area, these are described further below.

Box Model Sensitivity Studies

The four box model cases (0-3) are summarized in Table 3. Cases 0-2 use different constraints for the amount of aerosol surface area available for heterogeneous chemical reactions, and case 3 adjusts the gas phase kinetics of bromine reactions. The base case (case 0) used JPL kinetics and UHSAS measured surface area. Size specific particle concentrations for particles between 84 nm and 1 µm were measured by the UHSAS and were used to compute a surface area, assuming spherical particles. This is taken to be the minimum aerosol surface area available, because a previous optical closure study using AMAX-DOAS and High Spectral Resolution Lidar (HSRL) (Volkamer et al., 2015) found that the airborne UHSAS may underestimate particle size by about a factor of two for reasons that are currently not well understood. Examination of CONTRAST data confirms that this is again the case (Supplement, Fig. S3)

The first chemical sensitivity study (case 1) is identical to case 0, but used the measured UHSAS surface area multiplied by four, based on results of these optical closure studies. The rationale for case 1 is that heterogeneous and multiphase chemistry (uniformly represented using heterogeneous kinetics in the box model) can be determinative to the gas phase lifetime of Br_y reservoir species (i.e., HBr, and to a lesser extent also HOBr and $BrONO_2$). The fact that measured surface area is a lower limit has implications for heterogeneous reaction rates, bromine recycling and the BrO/Br_y ratio, and case 1 provides the best estimate of the available aerosol surface area.

The second sensitivity study (case 2) explores the possible effect of ice particles on bromine partitioning. Even very low ice concentrations add significant surface area that has the potential to rapidly impact local chemistry. CDP and 2D-C measure super-micron sized particles, cloud droplets, and ice. Sparse ice particles present a sampling challenge, and measurements were used as qualitative indicators for the presence of ice. 2D-C sometimes detected the presence of ice under conditions when ice should have sublimed, which may be due to rapid gravitational settling of ice particles. There might be insufficient time for the gas phase Br_y partitioning to equilibrate to the surface area of such ice particles, and as a result case 2 likely indicates a lower limit of gas phase Br_y. Case 2 used an ice climatology constructed from GEOS-5 data (Molod et al., 2015) whenever 2D-C indicated the presence of ice. An additional sensitivity study (not shown) explored the potentially large surface area contribution from super-micron particles (not measured by UHSAS) that are visible in the CDP data at lower altitudes.

Finally, the third sensitivity study (case 3) used the Br_y kinetics suggestion of Kreycy et al. (2013) to represent the conversion of BrO and $BrONO_2$. This is mediated by the reaction BrO + NO_2 and the photolysis of $BrONO_2$. Kreycy et al. (2013) investigated BrO, O_3, and NO_2 concentrations in the polar stratosphere at sunset and found the measured variations with respect to solar zenith angle deviated from theory based on JPL kinetics (Sander et al., 2011). Their recommended modifications of

$k_{BrO+NO2,\ Kreycy} = 0.75 * k_{BrO+NO2,\ JPL}$ and $J_{BrONO2,\ Kreycy} = 1.27 * J_{BrONO2,\ JPL}$ are used only for our case 3. These changes are relevant only in stratospheric air, where $BrONO_2$ is a significant daytime reservoir species.

Box Model Heterogeneous Chemical Regimes

The following heterogeneous chemical regimes (HCR) are distinguished to evaluate partitioning among Br_y and BrO_x species:

HCR1 – low Surface Area density (SA): SA <2×10^{-3} cm^2/m^3. Partitioning among BrO_x and the reservoirs is well approximated as three independent (gas phase) equilibria of BrO_x with the Br_y reservoir species HOBr, HBr, and $BrONO_2$. HBr is typically the major Br_y species, and the BrO_x/Br_y ratio is low (0.20 – 0.40). This regime is most relevant in the upper FT and convective TTL (all box-model cases). These regions are further characterized by low O_3 and high J_{BrO}; and as a result Br atoms make up near half or the majority of BrO_x. The BrO/Br_y ratio is typically <0.15, Br_y estimates are moderately sensitive to the available SA.

HCR2 – moderate SA: $2\times10^{-3} < SA < 1\times10^{-2}$ cm^2/m^3. Heterogeneous reactions have the potential to shift the HBr/BrO_x equilibrium dramatically. HBr does not readily photolyse, and reacts slowly with OH radicals to form BrO_x in the gas phase. As a result, heterogeneous reactions are the dominant loss process for HBr. Further, HOBr and O_3 can facilitate the heterogeneous conversion of condensed phase bromide back into the gas phase. In this regime HBr/Br_y is strongly sensitive to the available SA as well as the rates of heterogeneous reactions. The BrO_x/Br_y ratio can increase rapidly from 0.20 to 0.70 (depending strongly on SA, see Sect. 3.3 and Fig. S4). The upper limit of BrO_x/Br_y is sensitive to both $[H_2O]$ vapor and $[O_3]$, which control the concentration of HO_x. The abundance of HO_x is important due to the reactions $BrO + HO_2 \rightarrow HOBr + O_2$, and to a lesser extent $Br + OH \rightarrow HOBr$ and $Br + HO_2 \rightarrow HBr + O_2$. HCR2, which is relevant in the mid/upper FT and convective TTL (base case) and the upper FT and the convective TTL (case 1). The SA which accompanies the presence of ice (case 2) is such that HCR2 is eliminated. The BrO/Br_y ratio is strongly correlated with SA, changing by up to a factor of four between cases 0 and 1. O_3 and H_2O concentrations and changes to J_{BrO} over this regime in the FT and TTL modulate BrO/Br_y between 0.14 and 0.40 (see Fig. 5 below).

HCR3 – high SA: SA > 1×10^{-2} cm^2/m^3. Heterogeneous reactions have the potential to eliminate HBr as a meaningful gas phase Br_y reservoir. HOBr is the main Br_y reservoir species. In the HCR3 regime, BrO_x/Br_y is insensitive to SA, as gas phase reactions become limiting, and typically varies between 0.20 and 0.50. Further increasing SA, such as by including supermicron particles measured by the CDP, does not modify the chemistry. This regime is relevant from the surface to the lower FT, and in the aged TTL/stratosphere (case 0), surface to mid FT and aged TTL/stratosphere (case 1), and in the entire model atmosphere (case 2). In the troposphere, BrO/Br_y increases with altitude (from 0.15-0.25 near the surface to 0.45 - 0.50 in the mid FT), due to decreasing humidity and O_3 concentration (molec cm^{-3}), as well as the increasing value of J_{HOBr} with altitude. In the aged TTL, low humidity, low oxygenated volatile organic compound (OVOC), and high O_3 give rise to $BrO/Br_y > 0.35$. In the stratosphere, $BrONO_2$ becomes a significant Br_y reservoir species, and caps the BrO/Br_y ratio near 0.50.

2.3.2 CAM-Chem

The 3-D chemistry climate model Community Atmospheric Model with Chemistry (CAM-Chem) is described in (Lamarque et al., 2012). CAM-Chem includes all of the physical parameterizations of CAM4 (Neale et al., 2013) and a finite volume dynamical core (Lin, 2004) for the tracer advection. In the present configuration, meteorological analysis (from GEOS-5) specific to the observational periods are used to constrain the meteorological fields (horizontal wind components and temperature) in CAM-Chem. The horizontal resolution is 0.9°×1.25° and vertical resolution of 52 levels is includes full coverage of the troposphere and stratosphere, with a full representation of tropospheric and stratospheric chemistry. The VSL version used here includes geographically-distributed and time-dependent oceanic emissions six bromocarbons ($CHBr_3$, CH_2Br_2, CH_2BrCl, $CHBrCl_2$, $CHBr_2Cl$, CH_2IBr) as well as an additional source of inorganic bromine and chlorine in the lower troposphere due to sea-salt aerosol (SSA) dehalogenation (Fernandez et al., 2014; Ordóñez et al., 2012; Saiz-Lopez et al., 2012). In particular, it considers heterogeneous processes for halogen species on a variety of surfaces including uptake and recycling of HBr, HOBr, and $BrONO_2$ on ice-crystals and sulfate aerosols. The importance of these reactions, as well as the contribution from each independent VSL and sea-salt source to the halogen burden of SG and PG species in the TTL are discussed in (Fernandez et al., 2014). CAM-Chem output was used to examine how well modeled coupled chemistry and dynamics captured the BrO observations of the AMAX-DOAS and Br_y inferred by the box model.

2.3.3 GEOS-Chem

GEOS-Chem (Bey et al., 2001) is a global 3-D model of atmospheric composition driven by assimilated meteorological observations from the NASA Global Modelling and Assimilation Office (GMAO). GEOS-Chem is driven by GEOS-FP meteorological data. In this study, GEOS-Chem was used to simulate the coupled effect of bromine chemistry with other physical and chemical processes, and to test how well it captures BrO measured by AMAX-DOAS and Br_y inferred by the box model. Stratospheric concentrations (monthly and diurnally varying) of Br_y are taken from a GEOS-CCM simulation (Liang et al., 2010). Halogen chemistry in the model from Parrella et al. (2012) as referenced in Wang et al. (2015) has been updated (Schmidt et al., 2016; Sherwen et al., 2016, 2017a) and now includes more extensive heterogeneous chemistry including reactions on ice crystals and cross-halogen coupling. These changes have led to a reduction in modeled HBr/Br_y as well as Br_y washout, leading to an increase in BrO_x/Br_y (Schmidt et al., 2016).

3 Results

3.1 Bromine Vertical Profiles

The locations of the vertical profiles are shown in Fig. 1, with details as follows: 1) descent from RF03 on 17 January, 2014 starting at 01:11 UTC at 9.0°N, 150.1°E at 12.2 km heading southeast, and ending at 01:40 UTC at 7.4°N, 151.8°E at 300 m over the Chuuk atoll, 2) ascent from RF04 on 19 January, 2014 heading due north at 133.0°E starting at 03:20 UTC at 9.2°N at 400 m and ending at 03:38 UTC at 12.2°N at 13.2 km, and 3) ascent from RF07 on 29 January, heading due west at 1.1°N starting at 03:23 UTC at 150.5°E at 500 m and ending at 03:53 UTC at 147.6°E at 13.8 km. These profiles represent conditions that are well suited to profile retrievals (SZA<70°, mostly cloud free) and contain at last two measurements in each 500 m altitude bin.

Measured BrO profiles are shown in the left-most panels of Fig. 2 and exhibit significant variability. BrO concentrations in the lowest 500 m were 1.0±0.5 ppt (RF03, Fig. 2a), 1.7±1.2 ppt (RF04, Fig. 2e), and <0.5 ppt (RF07, below detection limit, Fig. 2i). The uncertainty reflects the overall retrieval error here. The BrO variability was further characterized during level flight at low altitude following the RF03 descent over Chuuk and prior to the RF04 ascent. Mean mixing ratios retrieved from these data varied between 0.9-1.6 ppt BrO (RF03) and 1.6-4.4 ppt BrO (RF04). The higher value is not the result of a single outlier, but rather represents the maximum of several minutes of data acquisition, for which retrieved BrO is > 3.5 ppt. These results suggest that BrO heterogeneity in the lowest 500 m is likely significant at both local and regional scales. At these altitudes AMAX-DOAS spectra average over path lengths of 5 km horizontally, which eases the comparison with model predictions on regional scales.

There is significant BrO variability also in the transition layer (TL: 0.5-2 km), where BrO mixing ratios are elevated relative to the lower FT. The mean mixing ratios below 2 km are 0.9±0.4 ppt (RF03), 1.3±0.6 ppt (RF04) and 0.7±0.7 ppt (RF07). Unless otherwise noted, errors bars reflect the variance of atmospheric variability, and retrieval errors with statistical leverage added in quadrature. The profiles also show variable structure through the lower and middle FT (2.0 - 9.5 km), with mean BrO mixing ratios of 0.5±0.3 ppt (RF03), 1.0±0.3 ppt (RF04), and 0.5±0.2 ppt (RF07). In the upper FT and lowermost TTL (tropospheric air > 9.5 km), the mean BrO mixing ratios are 0.4±0.2 ppt (RF03) and 0.6±0.2 ppt (RF07).

The distribution of Br_y species was modeled for each altitude grid point separately for the three profiles. Figure 2 show results for cases 0 and 2. Here we present a discussion of case 0, leaving the other cases for the sensitivity study presented in Sect. 3.3. The profiles contain significant structure in aerosol SA, humidity, and O_3, which can be characterized in the context of the HCR1-3 regimes outlined in Sect. 2.3.1. HCR1 applies at altitudes above 7-10 km, while HCR3 dominates in the lower troposphere. The chemistry transitions from HCR3 to HCR2, and from HCR2 to HCR1, occur at 8.0 km and 10.0 km (RF03), 6.0 km and 7.0 km (RF04), and 5.5 km and 9.0 km (RF07), respectively. Broadly, in the lower FT (< 6.5 km) the SA is high enough to remove HBr in the box model. As a consequence, Br_y estimates are insensitive to further increases in SA, and the BrO/Br_y ratio is solely determined by gas-phase chemistry. In contrast, between 6.5 and 13.5 km the inferred Br_y is sensitive to assumptions about the available SA and heterogeneous chemistry (see Table S3). The mean ratio BrO/Br_y from the surface through the mid FT (< 9.5 km) is 0.24±0.05 (RF03), 0.18±0.03 (RF04), and 0.21±0.05 (RF07). The inferred Br_y in the MBL and TL (< 2.0 km) is 4±2 ppt (RF03), 9±3 ppt (RF04) and 4±3 ppt (RF07). All three flights have Br_y minima in the lower to mid FT (2.0 - 9.5 km), for which the mean Br_y is 2±1 ppt (RF03), 4±1 ppt (RF04), and 2±1 ppt (RF07).

In the lower troposphere chemistry resides in the HCR3 regime. There is significant variability in the BrO/Br_y ratio, which can be explained by the factors most important to HCR3 partitioning: humidity and O_3. Average water vapor mixing ratio below 6.5 km is 1.08% (RF03), 1.28% (RF04) and, 0.97% (RF07) and the mean O_3 is 30 ppb (RF03), 25 ppb (RF04), and 33 ppb

(RF07). The higher humidity favors HOBr over BrO_x in RF04 compared to RF03 and RF07. Lower O_3 in RF04, particularly in two filaments with O_3 below 20 ppb between 1-2 km and 3-4 km, further compounds the difference with the other two flights and drives BrO/Br_y to even lower values.

In the mid FT chemistry resides in the HCR2 regime. The decreasing SA with altitudes allows HBr to be an increasingly important reservoir (i.e., heterogenous processing of HBr becomes slow) and drives down the computed value of BrO/Br_y. In parallel, the trends in HCR3 chemistry from below continue in the mid FT, i.e., BrO_x is increasingly favored over HOBr as $[H_2O]$ decreases and J_{HOBr} increases, and the Br/BrO ratio shifts toward Br as low temperatures and low $[O_3]$ slow $Br + O_3 \rightarrow BrO + O_2$, and J_{BrO} increases with altitude. Overall, BrO/Br_y remains roughly constant at 0.30±0.07 (RF03), 0.23±0.02 (RF04), and 0.17±0.03 (RF07). The mean surface area in RF03 is ~3 times that in RF04 and RF07, driving the higher average value of the BrO/Br_y ratio. The variability in BrO/Br_y in RF03 and RF07 is also driven by greater variability in SA, which is relatively constant at these altitudes in RF04.

HCR1 applies in the upper FT and TTL, where HBr is the primary reservoir species of Br_y. The BrO_x/Br_y ratio is low, almost constant in the box-model at these altitudes, with values of 0.10±0.01 (RF03) and 0.09±0.02 (RF07). The BrO_x-reservoir equilibria are relatively stable; changes in the BrO/Br_y ratio result from displacements of the Br/BrO partitioning. Observed mixing ratios of O_3 are low – decreasing from 26 ppb at 9 km to 18 ppb at 12.5 km in RF03, and varying between 23 and 24 ppb over the same altitudes in RF07, before dropping to 18 ppb at 14 km. Temperature decreases from 248 K at 9 km to 223 K at 12.5 km in RF03 and from 250 K to 222 K over the same altitudes in RF07 then further to 213 K at 14 km. Measured J_{BrO} continues to increase with altitude. In the upper FT the Br/BrO ratio is ~1, while in the TTL BrO is reduced to as little as 28% of BrO_x, yet BrO remains well above the DOAS detection limit. Note that BrO is flat or only mildly increasing in the upper FT and TTL. However, the decrease in BrO/Br_y drives an increase in Br_y from 2.1 ppt at 9 km to 5.6 ppt at 12.5 km, with a maximum of 7.2 ppt Br_y at 11 km (RF03), and 3.6 ppt at 9 km to 12.8 ppt at 14 km (RF07).

3.2 TTL and LS

The BrO mixing ratios during flight track legs flown at a level altitude were retrieved using the parameterization technique outlined in Dix et al. (2016), as described in Sect. 2.1.2. Figs. 3 and S5 show a number of tracers used to define the TTL and LS during RF06 and RF15. These are simplified into four regimes with simple, single variable definitions that allow separation for ease of examination. The LS is defined as air above 12.5 km and O_3 > 200 ppb, and the TTL is above 12.5 km and O_3 < 200 ppb.

As can be seen in Fig. 3, the LS defined this way is poleward of the jet stream, and is characterized by consistently low H_2O and CO, and high O_3 varying between 200 ppb and 900 ppb. The transition from the TTL to the LS is marked by greatest O_3, above the levels found elsewhere in the stratosphere. CFC-11, not shown in Fig. 3, is below 230 ppt in the stratosphere. The lower stratosphere is further divided into the middleworld LS and overworld LS. The division from Hoskins (1991) of 380 K potential temperature (θ) is slightly modified to 377 K, to obtain two contiguous regions (top panel, Fig. 3). The transition from the middleworld to the overworld is also marked by high O_3, much like the LS entrance and exit.

The TTL is divided into the convective TTL defined as air masses with $H_2O/O_3 > 0.1$ ppm/ppb and the aged TTL where $H_2O/O_3 < 0.1$ ppm/ppb. Figure S6 compares this classification to tracer-tracer classifications of the TTL from other works. The left panel uses the definition from Pan et al. (2014) as proxy for the TTL: $[H_2O] > [H_2O]_{stratospheric}$, and $[O_3] > [O_3]_{tropospheric}$. Using this definition, the convective TTL as defined here includes high altitude tropospheric air and the aged TTL includes stratospheric air. The right panel correlates [CO] and $[O_3]$ examining CONTRAST RF15, as done in Chen et al. (2016). The aged TTL as defined in this work is nearly equivalent to the TTL-LMS transition defined in Chen et al., [CO] is correlated with $[O_3]$ with a slope of -0.4. Exceptions to this are that portions of the convective TTL, and a mid FT filament (RF07), fall on the same line (would be TTL-LMS in Chen), and portions of the aged TTL (RF06, RF15) organize as parallel lines with slopes of -0.03, which would classify as stratospheric in Chen.

As the tracer-tracer correlations make apparent, the aged TTL is characterized by O_3, H_2O, and CO changing in concert. There is no consistent correlation between $[O_3]$ and $[H_2O]$, though both vary significantly. In contrast, there is a consistent strong inverse correlation between $[O_3]$ and [CO]. The aged TTL is also characterized by concentrations of fine aerosol SA sufficient for HCR3 (or marginal HCR2).

As the name suggests, the convective TTL is influenced by recent convection, and includes high altitude air which is essentially tropospheric. Relative to the aged TTL is characterized by high H_2O and corroborated by elevated CO, low O_3, and low θ. Convective air masses are observed for sufficiently brief periods to be averaged over by AMAX observations. Fig. S5 shows a region which was only observed in RF06 termed the convective TTL transition ($0.1 < H_2O/O_3 < 0.3$). Using the H_2O/O_3 criterion this region is in the convective TTL, and tracer-tracer analysis corroborates an essentially tropospheric character. However, it shows no signs of recent convection, and concentrations of O_3, CO, and H_2O are similar to the aged TTL; hence the name TTL transition.

Bromine in the Jet-Crossing Case Studies

Comparing Figs. 4 and S7 to Fig. 2, the mean BrO 0.53±0.08 ppt (RF06) and 1.01±0.08 ppt (RF15) in air recently impacted by convection ($H_2O/O_3 > 0.3$ ppm/ppb) was similar to that observed at the highest altitudes in RF03 and RF07. Chemically Br_y partitioning was characterized as HCR1 (see Sect. 2.3.1), HBr dominated Br_y, and Br made up the majority of BrO_x. This drove BrO/Br_y down to 0.12±0.01 (RF06) and 0.13±0.03 (RF15) (compared to 0.10±0.01 at 12.5 km in RF03 and 0.09±0.02 at 14.0 km in RF07). The inferred Br_y in turn was 4.3±0.5 ppt and 7.9±1.3 ppt for RF06 and RF15 in the TTL influenced by recent convection.

Portions of the convective TTL nearer to the aged TTL, including the convective TTL transition (see Sect. 3.2) in RF06, had more BrO, 0.9±0.1 ppt (RF06) and 1.1±0.5 ppt (RF15). This region included a rapid increase in aerosol surface area and ozone as the aircraft moved into lower stratospheric air. The increased SA lead to a transition from HCR1 to HCR2; however, the higher O_3 in the TTL gives rise to a higher BrO/Br_y compared to that of the mid and upper FT. Overall, BrO/Br_y rose (RF06: 0.18±0.05; RF15: 0.30±0.12) and more than compensated for the increase in BrO, and as a result Br_y stayed largely flat at 4.2±0.6 ppt (RF06) and 4.4±0.5 ppt (RF15).

Moving to the aged TTL in Figs. 4 and S7, BrO concentrations were elevated relative to the convective TTL (1.0±0.2 ppt RF06 and 1.6±0.1 ppt RF15). The greatest BrO mixing ratios in RF15 were observed nearest the stratosphere, since RF06 never reached the stratosphere this may in part explain the higher mean in RF15. Elevated O_3 caused BrO to dominate BrO_x. However, the high O_3 coupled with increased NO_2 caused $BrONO_2$ to make up to 20% of daytime Br_y for case 0, while $BrONO_2$ is converted to HOBr for the cases including efficient recycling. This had a limiting effect on BrO_x/Br_y as illustrated in Fig. S4. Chemical uncertainty in these air masses is driven by this increase in $BrONO_2$, see also Sect. 3.3. BrO/Br_y is high in the aged TTL (0.466±0.008 in RF15), giving an inferred Br_y of 2.0±0.3 ppt Br_y (RF06) and 3.49±0.17 ppt (RF15). A contributing factor to this difference may again be that the highest Br_y values in RF15 are observed nearest the stratosphere a region that RF06 did not sample.

BrO was observed to rise rapidly upon entering the stratosphere during RF15, i.e., from 1.97±0.12 ppt to 2.90±0.16 ppt in the middleworld. Though the middleworld changes in BrO paralleled changes in O_3, but Br_y partitioning could not explain these changes. Instead, the BrO/Br_y ratio was rather constant at 0.44±0.03. In the middleworld O_3 and NO_2 mixing ratios were both higher than in the aged TTL, which caused $BrONO_2$ to be competitive with HOBr as a daytime reservoir species. Consequently the modeled BrO/Br_y ratio is suppressed with increasing O_3, which is consistent with Fernandez et al. (2014). Figure S4, illustrates that the magnitude of this suppression is strongest when SA is high, as is the case in the middleworld LS.

Following the climb into the overworld at the northern most point, the mean BrO slightly increased to 3.15±0.13 ppt, and the largest mixing ratio of 3.35 ppt BrO (5 minute average, 3.78 ppt is the 30 s maximum) was observed. Chemically, conditions were similar to the middleworld, $BrONO_2$ essentially replaced HOBr as a reservoir for Br_y, and the BrO/Br_y ratio remains flat. The small variations in BrO were mirrored by corresponding variations in BrO/Br_y leading to consistent Br_y of 7.2±0.6 ppt, without any overall trend in the overworld.

3.3 Box Model Sensitivity Studies

The BrO-inferred Br_y estimates from the box model sensitivity studies (Table 3, Sect. 2.3.1) are summarized in Table 4. For detailed results from each model case see Table S3. The higher SA of case 1 leads to higher BrO/Br_y ratios that translate into lower estimates of Br_y (by up to a factor of four) in the upper FT and TTL. Figure 5 illustrates the effect of adjusting the measured SA by UHSAS on BrO/Br_y (for sensitivity of BrO_x/Br_y see Fig. S4). The impacts on the inferred Br_y is further apparent in Figs. 7 and S8. At 11 km, the Br_y inferred from case 1 changes from 6 ppt Br_y (case 0, grey) to 3 ppt Br_y (case 1, red). The sensitivity in the inferred Br_y is largest in air masses in the upper FT and TTL which are in HCR1 and HCR2, and hence sensitive to aerosol SA. Assumptions about reaction probabilities on surfaces, γ also play a role; SA and γ are convoluted and the product of SA × γ determines many heterogeneous reaction rates. The box model does not represent washout, however, this too can be convoluted with SA and γ, as the total Br_y burden in the FT and above is the net result of the competition between Br_y sources, washout, and the heterogeneous reaction rates for $BrONO_2$, HBr and HOBr.

When moving from case 0 to case 1, the altitude at which HCR3 shifts into HCR2 increases to higher altitudes, i.e., from 8.0 to 9.5 km (RF03), 6.0 to 8.0 km (RF04), and 5.5 to 9.5 km (RF07). The transition from HCR2 to HCR1 is not encountered in case 1 during RF03 and RF04, but it is observed for RF07 (the altitude of this transition shifts from typically 10.5 (case 0) to 12.0 km (case 1)). The convective TTL during both jet-crossing flights (which in case 0 is HCR1 and HCR2) shifts to HCR2 and HCR3 in case 1, with implications for the sensitivity to infer gas phase Br_y. The remaining HCR2 air masses are those with the greatest H_2O/O_3, i.e. those that have the most convective character and are most similar to the upper FT.

In case 2, ice greatly increases SA and has the further effect of converting $BrONO_2$ to HOBr. The presence of ice shifts heterogeneous chemistry to higher SA than shown in Figs. 5 and S4, and all air moves into the HCR3 regime in the box model. Case 2 has no effect on Br_y estimates at altitudes below 6 km (no ice observed), and no significant effect in the aged TTL. A minor effect to increase the BrO/Br_y ratio is visible in the upper FT and convective TTL in Fig. S8 (cyan whiskers). Note that within Case 2 BrO_x represent more than 80% of total Br_y, a fraction that increases as ambient ozone is reduced (Fig. S4). Under these conditions, the ratio Br/BrO > 1 and atomic bromine becomes the dominant Br_y species within the convective TTL (see Fig.2c,k and Fig. 4c). Thus, current box modelling results constrained with CONTRAST measurements and effective heterogeneous recycling are consistent with the proposed tropical rings of atomic halogens, where atomic bromine dominates inorganic bromine partitioning under the low ozone and ambient temperatures prevailing in the tropical TTL (Fernandez et al., 2014; Saiz-Lopez and Fernandez, 2016).

Kreycy et al. 2013, proposed that $BrONO_2$ is relatively unstable, and recommend increasing $BrONO_2$ photolysis and decreasing $BrONO_2$ formation. Because ice similarly disrupts $BrONO_2$ both effects are included in case 3 to determine the maximum combined effect on $BrONO_2$. No discernible impact on Br_y is found for tropospheric air masses, and only a minor impact is visible in the stratosphere for the case studies of this work. The impact on Br_y partitioning in the stratosphere is visible in Fig. 4, however the impact on BrO/Br_y can be difficult to discern. In the TTL BrO/Br_y increases by 2.9-6.5% over case 0, and 1.5-3.1% over case 2. The impact is greater in the aged TTL and hence greater in RF15 than RF06. The effect in the stratosphere is an increase of BrO/Br_y by 5.5-7.1%, leading to a slight reduction in the inferred Br_y. Since BrO/Br_y is ~50%, the change in leverage is minimal, and the effect on inferred Br_y is not significant.

4 Discussion

4.1 Tropospheric BrO and Br_y

The overall median tropospheric BrO and Br_y profiles are shown in Fig. 6. These profiles exhibit a C-shaped profile shape characteristic of convective transport (Kley et al., 1996; Pan et al., 2017). To our knowledge these are the first observations of C-shaped profiles for tropospheric inorganic bromine species (MBL into the upper FT). The data are further summarized in Table 4. The median BrO profile decreases with altitude, from an MBL median of 1.72 ppt to a minimum around 0.5 ppt in the mid/upper FT, and increases again in the convective TTL, see Fig. 6 and Table 4.

The trends in Br_y for the simulation case 1 (red in Fig. S8) are similar to those for BrO. Br_y decreases from a MBL median of 13.8 ppt toward a minimum of 1.6 ppt in the mid FT, where Br_y is roughly constant with altitude. Br_y begins to increase in the uppermost portion of the upper FT and reaches a local maximum in the convective TTL of 3.3 ppt. However, unlike BrO (which increases from the convective TTL to the aged TTL) gas phase Br_y decreases from the convective TTL to the aged TTL, as is further discussed in Sect. 4.2 below (see also Fig. 7).

The box model sensitivity study medians are summarized in Table 4, and a comprehensive summary for all cases is given in Table S3. As seen in Fig. S8, a common feature to all model results is the C-shaped profile in Br_y, which is most pronounced in case 0, and least pronounced in case 2. The estimated Br_y concentration is most sensitive in the mid and upper FT, as well as in the convective TTL, and responds sensitively to the available SA and assumptions about heterogeneous reaction rates that recycle bromine. Case 0 (grey in Fig. S8) has significantly more Br_y in all three regions, but especially in the upper FT, where the inferred Br_y is 3-5 times higher in case 0 compared to cases 1 and 2. Indications of an artificial high-bias in Br_y for case 0 arise from a step change in the Br_y vertical distribution between 12 and 13 km altitude (case 0). No similar step change is observed for model cases 1 and 2, which show a gradual and smooth Br_y increase from the mid FT into the convective TTL. A previous optical closure study had revealed a low-bias in the UHSAS measured aerosol SA for reasons that are currently not well understood (Volkamer et al., 2015), which can lead to high-bias in Br_y in the upper FT unless corrected (Wang et al., 2015). The step change in the Br_y profile for case 0 shown in Fig. S8, and the continuous behavior exhibited in case 1, provides corroborating evidence that SA is more accurately represented in case 1. The median Br_y from case 1 has thus been listed in Table 4. Case 2 (cyan in Fig. S8) has overall less Br_y in the mid and upper FT, and TTL than case 1, and likely represents a lower limit for Br_y. If heterogeneous bromine recycling on the much larger ice SA is as effective as on aerosols, the potential impact of ice shifts the Br_y minimum from the mid FT into the upper FT. The differences in Br_y from cases 1 and 2 are smaller than 0.5 ppt in the convective and aged TTL, as is indicated by the 1st quartiles in Table 4, and further discussed in Sect. 4.2.

4.2 Br_y structure in the UTLS

Figure 7 shows Br_y against different tracers of the stratosphere and troposphere. Colored points show case 1, grey squares case 0, and grey triangles case 3. Figure 7a has vertically decreasing CFC-11 as an indicator of stratospheric photochemical processing, Fig. 7b, shows increasing θ indicating the stable vertical positions of different air masses locally, and Fig. 7c shows decreasing H_2O/O_3 on a logarithmic scale as an indicator to increasing stratospheric and decreasing tropospheric character. Consistently in Fig. 7 there is significant variability in the Br_y across the tropospheric-stratospheric interface. A distinct minimum in gas phase Br_y is visible in the aged lower TTL, and Br_y increases both towards lower and higher altitudes, i.e., with decreasing CFC-11 (Fig. 7a), increasing θ (Fig. 7b), and decreasing H_2O/O_3 ratio (Fig. 7c). Figure 7a shows the correlation of Br_y against CFC-11, a tracer of photochemical age. CFC-11, similar to long-lived bromocarbons, does not photolyse significantly in the troposphere, where the mixing ratio is constant at about 237 ppt (Carpenter and Reimann et al., 2014). TTL data has CFC-11 levels that are tropospheric or very near tropospheric, and the convective and aged TTL cannot be separated by CFC-11. This suggests that the aged TTL contains mostly tropospheric air, and contributions from the stratosphere are small. The photochemical liberation of Br_y from bromocarbons, including VSLS, in the aged TTL is indistinguishable from the variance of the convective inputs. CFC-11 decreases in the middleworld, consistent with the observed Br_y increase. This matches the expected behavior as long lived bromocarbons and possibly VSLS are photolysed along with CFC-11, liberating

Br_y. However, this correlation does not extend into the overworld, where despite greater depletion of CFC-11, the Br_y expected to result from bromocarbon photolysis is not observed. Notably, gas phase Br_y does not include aerosol bromide, which is unconstrained by CONTRAST observations. Gas phase Br_y is not a conservative quantity, rather it is a lower limit of total bromine in the UTLS.

Taking [CFC-11] = 237 ppt as the definition of the tropopause, the gas phase inorganic Br_y injected into the stratosphere is found to be 2.6±0.6 ppt Br_y for case 1. The slope of the Br_y - CFC-11 correlation fitted for all data is 0.15±0.03. The middleworld points with 210 ppt < [CFC-11] < 230 ppt show the clearest correlation, with a slope of 0.22±0.01. Assuming no other source or sink for Br_y, this indicates that on average CBr_y liberates Br_y at 0.15 (and up to 0.22) the rate of CFC-11 decay in the stratosphere. Modeling of sea-salt derived Br_y in the troposphere without any contribution from organics suggests such sources are responsible for 2±1 ppt Br_y in the TTL (Long et al., 2014). Additionally, previous CAM-Chem sensitivity studies determined that the contribution of sea-salt derived bromine to the lower TTL was small (< 0.5ppt) for the global-mean TTL (equivalent to the aged TTL here), but represented more than 3.6 pptv within strong convective regions such as the tWPO (equivalent to the convective TTL here) (Fernandez et al., 2014). The difference between the regions in CAM-Chem is sensitive to the balance between recycling and washout process, which are uncertain. Thus, it is possible that the majority of the inorganic bromine in the TTL is related to sea-salt bromine sources. This is consistent with reports of underestimated Br_y in lower stratospheric air in the SH subtropics which suggest an underestimation of stratospheric injection of 1.2 ppt Br_y when neglecting sea-salt source (Wang et al. 2015).

Examining Figure 7b, a similar story emerges. Potential temperature (θ) quite effectively separates the different air mass types (Hoskins, 1991). The LS has θ greater than 370K, with the overworld defined here as $\theta > 377$ K. There is a Br_y minimum of 2.3±0.5 ppt between θ of 360K and 365K. Then, Br_y increases with θ through the remainder of the aged TTL and the middleworld. In the overworld, Br_y is roughly constant with respect to θ, as it is versus CFC-11, and largely independent of the assumptions about the kinetics of $BrONO_2$ (compare blue and grey triangles in Fig. 7). We conclude that the Br_y minimum in the aged TTL is robust.

Figure 7c shows Br_y versus the H_2O/O_3 ratio. This panel more fully separates the aged and convective TTL and highlights the decrease in Br_y in the aged TTL. Br_y is nearly constant at 2.7±0.9 ppt for values of H_2O/O_3 characteristic of the aged TTL; Br_y increases in the more humid and lower O_3 air at lower altitudes, as well as in the stratospheric middleworld. The H_2O/O_3 ratio is found to be the best tracer for the higher Br_y in the convective TTL; it also holds the most (albeit still limited) potential for capturing any trend in the overworld. While panels A and B do not reveal any trend for Br_y versus either CFC-11 or θ in the overworld, the fitted trend of Br_y versus H_2O/O_3 in panel C is neither different from zero, nor statistically different from the trend in the middleworld.

4.3 Comparison with Global Models

Observed BrO and inferred Br_y in different portions of the atmosphere, as summarized in Table 4, are compared to output from GEOS-Chem and CAM-chem global models in Fig. 6. Table 5 compares the corresponding partial and total tropospheric BrO VCDs. Examining the latter, the observations have a median value of 1.65×10^{13} molec cm^{-2}, while CAM-chem predicts about 25% of this value (0.41×10^{13} molec cm^{-2}). GEOS-Chem without SSA source predicts 55% or 0.91×10^{13} molec cm^{-2}; the closest to the observed value is GEOS-Chem with the SSA source predicts 125% or 2.07×10^{13} molec cm^{-2}.

In the MBL the high concentrations of BrO observed and inferred Br_y are intermediate between the GEOS-Chem simulations including and excluding the SSA Br_y source. The 95th percentile trace of CAM-chem further illustrates that CAM-chem captures instances where BrO is above 4 ppt near the surface, though examination of the specific case studies reveals it does not match the location of observations. GEOS-Chem roughly reproduces the near surface vertical distribution of both BrO and Br_y with a TL partial VCD roughly twice that in the MBL (Table 5). For both BrO and Br_y when an SSA bromine source is excluded the decrease with altitude is greater than observed, while the reverse is true when the SSA source is included; some intermediate profile seems to best reproduce the observations.

In the free troposphere, the model simulations shown in Fig. 6 exhibit a high degree of variability. However, the variability in the observations spans a similar range. In the lower FT the median observed BrO is between 0.6 and 0.9 ppt, and is larger than predicted by global models, which show less than 0.5 ppt between 2 and 5 km (Fig. 6a). Continuing up through the FT, the CAM-chem median approximates the BrO and Br_y profile shapes reasonably well in the mid FT, but follows the low end of the BrO observations, while tracking median box modelled Br_y. As the 5th percentile and median CAM-chem profiles on Fig. 6 help illustrate CAM-Chem often has almost no BrO in the FT. GEOS-Chem shows significant enhancements of BrO and Br_y in the mid FT, which are not observed. In the upper FT, consistent with the results from Wang et al. (2015), a SSA source best reproduces the median BrO observations. However, excluding the SSA source from GEOS-Chem better reproduces Br_y, while CAM-chem with the SSA source underestimates Br_y.

In the TTL GEOS-Chem (with and without the SSA source) shows some increase in BrO and Br_y at the highest altitudes, but only after a minimum in the same region. CAM-chem does not show this increase in the median, though the 95th percentile makes transparent that elevated BrO is predicted in certain instances. CAM-chem includes an explicit representation of the stratosphere, and as a result captures more of the variability in the UTLS (not included in Fig. 5). Examination of CAM-chem model output versus θ (Fig. S9) reveals a gas phase Br_y minimum, albeit at lower θ (~350 K) and with less Br_y (1.2 ppt) than observed. As in Fig. 4, the CAM-chem output with highest Br_y are more consistent with observations.

Notably, while both BrO and Br_y are broadly consistent, partitioning of Br_y is different between the box model and global models. The greatest difference is for HBr, where the tropospheric column abundance differs by over a factor of fifteen over the total column, as shown in Table S2. Broadly, GEOS-Chem has more $BrONO_2$ and HBr, and less HOBr compared to the box model. When the SSA bromine source is excluded the BrO/Br_y ratio roughly matches as the different components cancel out (visible as the BrO and Br_y comparing similarly in Fig. 6a and 6b). Further, O_3 is slightly higher in GEOS-Chem than observed, resulting in a greater BrO/BrO_x. In CAM-chem however, Br_y partitioning is broadly similar to the box model, with the key exception of HBr. The larger amount of HBr in CAM-chem is responsible for the agreement in Br_y in the FT, despite underestimating BrO observations. GEOS-Chem with an SSA source also has substantially more HBr near the surface, significantly lowering the BrO/Br_y ratio. Notably, the additional HBr in GEOS-Chem falls off more rapidly with altitude than in CAM-Chem, suggesting that transport, recycling, and/or washout are different between the global models. These differences manifest differently in the TTL, where HBr falls off more rapidly in CAM-CHEM than in GEOS-Chem. As Table S2 highlights, only in the upper FT (HCR1) is HBr in the global models consistent with that in the box model. This further reinforces the strong impacts of uncertainties in HBr heterogenous chemistry when coupled to transport and washout.

4.4 Comparison with other studies

Tropospheric measurements of BrO and other Br_y species were obtained by two CIMS instruments over the tWPO during same period as the AMAX-DOAS measurements described above. The Georgia Tech CIMS (GT CIMS) was on the same GV platform as the AMAX-DOAS and measured BrO and Br_2+HOBr, with results summarized in Chen et al., 2016. There was no overlap between the tropospheric case studies presented here and those in Chen et al.; the CIMS had calibration challenges for early flights, while cloudy conditions precluded AMAX-DOAS retrievals for later flights. The Manchester University CIMS (MU CIMS) was aboard the British Aerospace 146 (BAe-146) aircraft as part of the Coordinated Airborne Studies in the Tropics (CAST) project (Harris et al., 2017). During CAST, the BAe-146 had a ceiling altitude of 9 km on flights between and out of Guam, Chuuk, and Palau (Koror) which are indicated on Fig. 1. The MU CIMS sampled the troposphere during CAST in broadly the same region as the tropospheric case studies presented for the AMAX-DOAS during CONTRAST. Measurements from the MU CIMS cover BrO, Br_2, BrCl, and HOBr, all reported separately (Le Breton et al., 2017).

A comparison of tropospheric data from the AMAX-DOAS and the two CIMS instruments is presented in Fig. S10. The GT CIMS has a detection limit of ~1 ppt for BrO, which is substantially higher than that of MU CIMS and AMAX-DOAS. The BrO measured by MU CIMS and AMAX-DOAS is below the GT CIMS detection limit >75-90% of the time for altitudes between 2 and 12.5 km. There are no GT CIMS measurements below 1 km, where AMAX-DOAS shows significant variability for BrO. While AMAX-DOAS mostly samples clear sky conditions, the GT CIMS was operating mostly during cloudy flights near convection. Such conditions favor the uptake of bromine into the condensed phase, and as a result the differences in the BrO measurements between these two instruments may in part reflect true differences in the sampled atmospheric conditions. The AMAX-DOAS and MU CIMS data generally agree for BrO in the altitude range from 3.5 to 9.0 km (Fig. S10a). The measured Br_y from MU CIMS (i.e., $BrO+2\times Br_2+HOBr+BrCl$) is in rather good agreement with Br_y inferred from AMAX-DOAS over the 3.5 to 9.0 km altitude range, providing support for the overall veracity of our study (Fig. S10b). There are no MU CIMS measurements above 9 km. In the TTL, the differences between the GT CIMS and AMAX-DOAS are not readily resolved. These discrepancies are unlikely explained by atmospheric variability, as is discussed below.

Both the AMAX-DOAS and GT CIMS operated concurrently aboard the GV during the RF15 case study, where elevated BrO was expected due to sampling of the overworld. CAM-chem suggests that there should be 1-2 ppt BrO just prior to entering the LS (01:15 UTC of Fig. 8), which is in excellent agreement with between 1.3 and 2.1 ppt BrO observed by AMAX-DOAS in the aged TTL. By comparison, the GT CIMS observes no significant BrO in the aged TTL. Just prior to the entry into the stratosphere, GT CIMS reported 0.48±0.58 ppt BrO, which is below the GT CIMS LOD (0.6-1.6 ppt during RF15 for BrO) (Chen et al., 2016), and significantly lower than both AMAX-DOAS and CAM-chem. In the LS, GT CIMS BrO rapidly increases to ~3.8 ppt BrO (averaged for 02:09-02:14 UTC). The AMAX-DOAS measurements also rise, but more modestly to 2.9 ppt during the same period. The discrepancies cannot be readily explained by horizontal inhomogeneity, the air probed by the AMAX-DOAS has near complete turnover within 12 minutes along the straight line flight path. Notably, the GT CIMS does not report data when [O_3] exceeds 480 ppb, owing to unrealistically high BrO that was measured, but is not trusted under such conditions. This data filter precludes a comparison of measurements in the remainder of the stratosphere.

First tropospheric BrO profiles had recently been measured from aircraft over the tropical Eastern Pacific, tEPO, during the TORERO field campaign (Volkamer et al., 2015). Tropospheric BrO VCDs from five case studies in pristine marine air showed significant variability ($0.5\text{-}3.0\times10^{13}$ molec cm^{-2}; Volkamer et al., 2015; Wang et al., 2015). Dix et al. (2016) examined the TORERO BrO dataset more fully, and found a campaign median tropospheric BrO VCD of 1.8×10^{13} molec cm^{-2} (this median excludes measurements below detection limit, and thus may be an upper limit). This is similar to the tropospheric BrO VCD of 1.6×10^{13} molec cm^{-2} measured over the tWPO in this study. However, there are important differences in the tropospheric BrO profile shape between the tEPO and tWPO. While we find 37% of the BrO below 2 km over the tWPO, no significant BrO had been observed in the MBL and TL over the tEPO during TORERO, where essentially all (>95%) BrO was located above 2 km in the FT (Dix et al., 2016; Volkamer et al., 2015; Wang et al., 2015). Decreasing BrO with altitude had previously been observed during the TORERO RF04 case study (Wang et al., 2015). The overall TORERO data set supports observations of decreasing BrO in the lower TTL. The campaign mean BrO was 1.86 ± 0.16 ppt (95 % CI, N = 162) at 13.5 km, and decreased to 1.38 ± 0.16 ppt BrO (95 % CI, N = 78) at 14.5 km. This is consistent with 0.9 to 1.2 ppt BrO in the TTL measured here. As noted in Dix et al. (2016), this decreasing BrO with altitude is highly significant during TORERO, and not inconsistent with results by Werner et al. (2017), as discussed below.

DOAS observations of BrO have also been reported from the Global Hawk platform at high altitudes (14 – 18 km) over the tWPO and tEPO (Stutz et al., 2017; Werner et al., 2017). The retrieved composite profile has BrO increase gradually from 0.7 ppt at 14.5 km to 1.1 ppt at 16.5 km, then more rapidly to 3.6 ppt at 18.5 km. The consistency between Br_y estimated from AMAX-DOAS of this work and the value of Br_y from Werner et al. is illustrated in Fig. 9. Werner et al. utilize a criterion of CH_4 = 1790 ppb to separate "young" air with more CH_4 and "old" air with less. Applying this same criterion to the CONTRAST DOAS data reproduces the TTL – LS separation. Utilizing the 10 K θ bins we find good agreement of Br_y in the TTL. In the LS, there is a mismatch wherein the Global Hawk and GV sampled old air at different θ. However, CH_4 concentrations span a similar range of 1690-1790 ppm indicating similar aging, and a general agreement for Br_y is also found in the LS. Notably, Werner et al. do not show a significant Br_y minimum in the TTL, probably due to the limited Global Hawk observations at θ < 355 K, where such a trend is most apparent in our data. Moreover, the LS Br_y measured in the Northern Hemisphere LS are consistent with the Br_y measured under double tropopause conditions in the Southern Hemisphere mid-latitude LS (Wang et al., 2015). Finally, CAM-chem shows good agreement with the Br_y from the box model in this work below 340 K and above 360 K. However, between 340 and 360 K the model predicts systematically lower Br_y than inferred. Navarro et al. (2016) have shown that the CAM-chem VSLS are consistent with CONTRAST observations. The PGI injection of VSLS, which are important to predicting Br_y profiles through the LS (Liang et al., 2010) are captured well by the model. The differences in the Br_y profile shape through the TTL are therefore unlikely to be related to VSLS alone, but most likely require additional processes.

Elevated concentrations of BrO (up to 3 ppt) in pristine air masses over the tEPO (Dix et al., 2016; Volkamer et al., 2015; Wang et al., 2015), and above Florida (Coburn et al., 2016) most likely reflect a variable influence of bromine sources from the lower atmosphere (e.g., SSA) downwind of marine convection (Long et al., 2014; Schmidt et al., 2016). Interestingly, the source region of the TORERO flights observed deep convective outflow that originated over the tWPO warm pool, in the area south of the CONTAST study area, where we observe significant BrO in the MBL consistent with SSA bromine sources. This is in contrast to low upper limits of <0.5 ppt MBL-BrO over the tEPO (Mahajan et al., 2012; Volkamer et al., 2015). Atmospheric models that represent sea-salt sources consistently predict several ppt BrO over tropical oceans (Long et al., 2014; Ordóñez et al., 2012; Schmidt et al., 2016; Yang et al., 2005). This conundrum is a primary reason why recent state-of-the-art models such as GEOS-Chem have decided not to represent the sea-salt source of bromine in their default configuration (Sherwen et al., 2016). The BrO profiles measured during this study suggests that SSA is a significant source of bromine over the tWPO. The reason for the low BrO over the tEPO MBL (Volkamer et al., 2015; Wang et al., 2015) deserves further study.

5 Conclusions

We identify a gas phase Br_y minimum in the aged TTL which is robust to assumptions regarding heterogeneous chemistry. Even taking into account the uncertainty spanned by the different box model cases, we find that the Br_y in the aged TTL is lower than in the convective TTL and in the upper FT (96% confidence), and that it is lower than in the lower stratosphere (LS) (>99% confidence). To our knowledge such a Br_y minimum has not previously been observed or hypothesized.

The Br_y minimum in the aged TTL is consistent with previous observations that BrO decreases from the upper FT into the lower TTL over the Eastern Pacific ocean (Dix et al., 2016), and with several recent Br_y estimates in the LS over the tropical Pacific (Wang et al., 2015; Stutz et al., 2017; Werner et al., 2017). Recent modeling of bromine does not explicitly predict such a minimum (Fernandez et al., 2014; Schmidt et al., 2016; Sherwen et al., 2016). However, modeling of iodine chemistry (which has some similarities) does predict a local minimum in gas phase inorganic iodine in the TTL (Saiz-Lopez et al., 2015), consistent with observations (Volkamer et al., 2015; Dix et al., 2016). The 2.7 ppt (2.4-3.0 ppt, 95% CI) gas phase Br_y inferred in the aged TTL minimum is a rough estimate of bromine PGI, and is in reasonable agreement with the latest WMO assessment of 1.1-4.3 ppt PGI (Carpenter and Reimann et al., 2014). Notably, a significant fraction of this Br_y may be SSA derived. It is currently unknown how much Br_y is transported into the stratosphere as aerosol bromide.

The currently available quantitative assessments of Br_y in the UTLS rely on measurements of gas phase Br_y species alone. The lack of quantitative aerosol bromine measurements leaves the total Br_y budget in the UTLS open to speculation. Indeed, aerosol measurements show a local maximum in aerosol halogen signals in the UTLS (Froyd et al., 2010; Murphy et al., 2006; Murphy and Thomson, 2000). Together with the Br_y minimum identified here, this suggests that the partitioning of bromine between the gas- and aerosol phases is significant, and cannot be ignored.

Our data provide strong evidence that a SSA derived bromine source is necessary to reproduce the observed profiles of BrO and Br_y near the surface and in the upper FT. CAM-chem, which includes a SSA bromine source, underestimates the BrO in the troposphere, but qualitatively reproduces the tropospheric BrO profile shape; similarly CAM-chem captures a Br_y minimum in the TTL, though not quantitatively. GEOS-Chem with SSA has discrepancies in the profile shapes but best matches the measured BrO VCD. Models diverge as to the fraction of gas phase Br_y that exists as HBr, especially in the lower atmosphere. This reflects uncertainties in the convective transport, uptake, recycling, and scavenging of gas-phase Br_y species (i.e., HOBr, HBr) and SSA-derived bromide, which are relevant for the inferred Br_y burden. Reducing these uncertainties will require comprehensive experimental field and laboratory work to close the total Br_y budget.

6 Data Availability

The AMAX-DOAS BrO data are available from the CONTRAST data archive: http://data.eol.ucar.edu/master_list/?project=CONTRAST. The CONTRAST data set is open for use by the public, subject to the data policy: https://www.eol.ucar.edu/content/contrast-data-policy. The archive contains aircraft and atmosphere state parameters, in situ measurements, flight videos, and links to the concurrent ATTREX and CAST campaign data archives and other ancillary measurements.

Author Contributions

E. Atlas, L. Pan, and R. Salawitch designed the CONTRAST research flights. S. Baidar, B. Dix, T. Koenig, and R. Volkamer performed CU AMAX-DOAS, measurements and analyzed data. D. Anderson, E. Apel, E. Atlas, N., Blake, J. Bresch, T. Campos, D. Chen, V. Donets, F. Flocke, S. Hall, T. Hanisco, S. Honomichl, R. Hornbrook, G. Huey, J. Jensen, R. Lueb, D. Montzka, M. Navarro, M. Reeves, D. Reimer, S. Schauffler, D. Tanner, K. Ullmann, A. Weinheimer, and G. Wolfe performed measurements, and performed data analysis for other instruments on the GV. C. Cuevas, M. Evans, R. Fernandez, D. Jacob, D. Kinnison, T. Koenig, J.-F. Lamarque, R. Salawitch, A. Saiz-Lopez, T. Sherwen, J. Schmidt, P. Wales, and S. Wang provided model data and analysis tools. T. Koenig and R. Volkamer wrote the manuscript with contributions from all authors.

Acknowledgements

We thank the CONTRAST team including pilots, technicians, forecasters, and scientists on the aircraft and on the ground particularly P. Romashkin and L. Lussier for making the campaign a success and this work possible. TK and RV would like to thank T. Bannan, M. Le Breton, and C. Percival for sharing their published data from the CAST field campaign. CONTRAST was funded by the National Science Foundation (NSF). R.V. acknowledges funding from NSF award AGS-1261740. The GV aircraft was operated by the National Center for Atmospheric Research's (NCAR) Earth Observing Laboratory's (EOL) Research Aviation Facility (RAF). CAST was funded by the National Environment Research Council.

References

Andrews, S. J., Carpenter, L. J., Apel, E. C., Atlas, E., Donets, V., Hopkins, J. F. R., Hornbrook, R. S., Lewis, A. C., Lidster, R. T., Lueb, R., Minaeian, J., Navarro, M., Punjabi, S., Riemer, D. and Schauffler, S. S.: A comparison of very short-lived halocarbon (VSLS) and DMS aircraft measurements in the Tropical West Pacific from CAST , ATTREX and CONTRAST, Atmos. Meas. Tech., 9(10), 5213–5225, doi:10.5194/amt-2016-94, 2016.

Apel, E. C., Hills, A. J., Lueb, R., Zindel, S., Eisele, S. and Riemer, D. D.: A fast-GC/MS system to measure C_2 to C_4 carbonyls and methanol aboard aircraft, J. Geophys. Res., 108(D20), 8794, doi:10.1029/2002JD003199, 2003.

Apel, E. C., Emmons, L. K., Karl, T., Flocke, F., Hills, A. J., Madronich, S., Lee-Taylor, J., Fried, A., Weibring, P., Walega, J., Richter, D., Tie, X., Mauldin, L., Campos, T., Weinheimer, A., Knapp, D., Sive, B., Kleinman, L., Springston, S., Zaveri, R., Ortega, J., Voss, P., Blake, D., Baker, A., Warneke, C., Welsh-Bon, D., de Gouw, J., Zheng, J., Zhang, R., Rudolph, J., Junkermann, W. and Riemer, D. D.: Chemical evolution of volatile organic compounds in the outflow of the Mexico City Metropolitan area, Atmos. Chem. Phys., 10(5), 2353–2375, doi:10.5194/acp-10-2353-2010, 2010.

Apel, E. C., Hornbrook, R. S., Hills, A. J., Blake, N. J., Barth, M. C., Weinheimer, A., Cantrell, C., Rutledge, S. A., Basarab, B., Crawford, J., Diskin, G., Homeyer, C. R., Campos, T., Flocke, F., Fried, A., Blake, D. R., Brune, W., Pollack, I., Peischl, J., Ryerson, T., Wennberg, P. O., Crounse, J. D., Wisthaler, A., Mikoviny, T., Huey, G., Heikes, B., O'Sullivan, D. and Riemer, D. D.: Upper tropospheric ozone production from lightning NOx -impacted convection: Smoke ingestion case study from the DC3 campaign, J. Geophys. Res. Atmos., 120(6), 2505–2523, doi:10.1002/2014JD022121, 2015.

Baidar, S., Oetjen, H., Coburn, S., Dix, B., Ortega, I., Sinreich, R. and Volkamer, R.: The CU Airborne MAX-DOAS instrument: Vertical profiling of aerosol extinction and trace gases, Atmos. Meas. Tech., 6(3), 719–739, doi:10.5194/amt-6-719-2013, 2013.

Bey, I., Jacob, D. J., Yantosca, R. M., Logan, J. A., Field, B. D., Fiore, A. M., Li, Q., Liu, H. Y., Mickley, L. J. and Schultz, M. G.: Global modeling of tropospheric chemistry with assimilated meteorology: Model description and evaluation, J. Geophys. Res. Atmos., 106(D19), 23073–23095, doi:10.1029/2001JD000807, 2001.

Bloss, W. J., Camredon, M., Lee, J. D., Heard, D. E., Plane, J. M. C., Saiz-Lopez, A., Bauguitte, .-B, Salmon, R. A. and Jones, A. E.: Coupling of HOx, NOx and halogen chemistry in the antarctic boundary layer, Atmos. Chem. Phys., 10(21), 10187–

10209, doi:10.5194/acp-10-10187-2010, 2010.

Boucher, O., Moulin, C., Belviso, S., Aumont, O., Bopp, L., Cosme, E., von Kuhlmann, R., Lawrence, M. G., Pham, M., Reddy, M. S., Sciare, J. and Venkataraman, C.: DMS atmospheric concentrations and sulphate aerosol indirect radiative forcing: a sensitivity study to the DMS source representation and oxidation, Atmos. Chem. Phys., 3(1), 49–65, doi:10.5194/acp-3-49-2003, 2003.

Le Breton, M., Bannan, T. J., Shallcross, D. E., Khan, M. A., Evans, M. J., Lee, J., Lidster, R., Andrews, S., Carpenter, L. J., Schmidt, J., Jacob, D., Harris, N. R. P., Bauguitte, S., Gallagher, M., Bacak, A., Leather, K. E. and Percival, C. J.: Enhanced ozone loss by active inorganic bromine chemistry in the tropical troposphere, Atmos. Environ., 155, 21–28, doi:10.1016/j.atmosenv.2017.02.003, 2017.

Cai, Y., Montague, D. C., Mooiweer-Bryan, W. and Deshler, T.: Performance characteristics of the ultra high sensitivity aerosol spectrometer for particles between 55 and 800nm: Laboratory and field studies, J. Aerosol Sci., 39(9), 759–769, doi:10.1016/j.jaerosci.2008.04.007, 2008.

Carpenter, L. J. and Reimann, S. (Lead Authors), Burkholder, J. B., Clerbaux, C., Hall, B. D., Hossaini, R., Laube, J. C., Yvon-Lewis, S. A., Blake, D. R., Dorf, M., Dutton, G. S., Fraser, P. J., Froidevaux, L., Hendrick, F., Hu, J., Jones, A., Krummel, P. B., Kuijpers, L. J. M., Kurylo, M. J., Liang, Q., Mahieu, E., Mühle, J., O ’Doherty, S., Ohnishi, K., Orkin, V. L., Pfeilsticker, K., Rigby, M., Simpson, I. J. and Yokouchi, Y.: Update on Ozone-Depleting Substances (ODSs) and Other Gases of Interest to the Montreal Protocol., Chapter 1 in Scientific Assessment of Ozone Depletion: 2014, Global Ozone Research and Monitoring Project – Report No. 55, World Meteorological Organization, Geneva, Switzerland, 2014.

Cazorla, M., Wolfe, G. M., Bailey, S. A., Swanson, A. K., Arkinson, H. L. and Hanisco, T. F.: A new airborne laser-induced fluorescence instrument for in situ detection of formaldehyde throughout the troposphere and lower stratosphere, Atmos. Meas. Tech., 8(2), 541–552, doi:10.5194/amt-8-541-2015, 2015.

Chance, K.: Analysis of BrO measurements from the Global Ozone Monitoring Experiment, Geophys. Res. Lett., 25(17), 3335–3338, doi:10.1029/98GL52359, 1998.

Chen, D., Huey, L. G., Tanner, D. J., Salawitch, R. J., Anderson, D. C., Wales, P. A., Pan, L. L., Atlas, E. L., Hornbrook, R. S., Apel, E. C., Blake, N. J., Campos, T. L., Donets, V., Flocke, F. M., Hall, S. R., Hanisco, T. F., Hills, A. J., Honomichl, S. B., Jensen, J. B., Kaser, L., Montzka, D. D., Nicely, J. M., Reeves, J. M., Riemer, D. D., Schauffler, S. M., Ullmann, K., Weinheimer, A. J. and Wolfe, G. M.: Airborne measurements of BrO and the sum of HOBr and Br_2 over the Tropical West Pacific from 1 to 15 km during the CONvective TRansport of Active Species in the Tropics (CONTRAST) experiment, J. Geophys. Res. Atmos., 121(20), 12,560-12,578, doi:10.1002/2016JD025561, 2016.

Coburn, S., Dix, B., Edgerton, E., Holmes, C. D., Kinnison, D., Liang, Q., ter Schure, A., Wang, S. and Volkamer, R.: Mercury oxidation from bromine chemistry in the free troposphere over the southeastern US, Atmos. Chem. Phys., 16(6), 3743–3760, doi:10.5194/acp-16-3743-2016, 2016.

Custard, K. D., Thompson, C. R., Pratt, K. A., Shepson, P. B., Liao, J., Huey, L. G., Orlando, J. J., Weinheimer, A. J., Apel, E., Hall, S. R., Flocke, F., Mauldin, L., Hornbrook, R. S., Pöhler, D., General, S., Zielcke, J., Simpson, W. R., Platt, U., Fried, A., Weibring, P., Sive, B. C., Ullmann, K., Cantrell, C., Knapp, D. J. and Montzka, D. D.: The NO_x dependence of bromine chemistry in the Arctic atmospheric boundary layer, Atmos. Chem. Phys, 15, 10799–10809, doi:10.5194/acp-15-10799-2015, 2015.

Danckaert, T., Fayt, C., van Roozendael, M., de Smedt, I., Letocart, V., Merlaud, A. and Pinardi, G.: QDOAS Software user manual v2.1, [online] Available from: http://uv-vis.aeronomie.be/software/QDOAS/QDOAS_manual_2.1_201212.pdf (Accessed 24 October 2016), 2012.

Deutschmann, T., Beirle, S., Frieß, U., Grzegorski, M., Kern, C., Kritten, L., Platt, U., Prados-Román, C., Puķı¯te, J., Wagner, T., Werner, B. and Pfeilsticker, K.: The Monte Carlo atmospheric radiative transfer model McArtim: Introduction and validation of Jacobians and 3D features, J. Quant. Spectrosc. Radiat. Transf., 112(6), 1119–1137, doi:10.1016/j.jqsrt.2010.12.009, 2011.

Dix, B., Baidar, S., Bresch, J. F., Hall, S. R., Schmidt, K. S., Wang, S. and Volkamer, R.: Detection of iodine monoxide in the tropical free troposphere, Proc. Natl. Acad. Sci., 110(6), 2035–2040, doi:10.1073/pnas.1212386110, 2013.

Dix, B., Koenig, T. K. and Volkamer, R.: Parameterization retrieval of trace gas volume mixing ratios from Airborne MAX-DOAS, Atmos. Meas. Tech., 9(11), 5655–5675, doi:10.5194/amt-9-5655-2016, 2016.

Dorf, M., Butler, J. H., Butz, A., Camy-Peyret, C., Chipperfield, M. P., Kritten, L., Montzka, S. a., Simmes, B., Weidner, F. and Pfeilsticker, K.: Long-term observations of stratospheric bromine reveal slow down in growth, Geophys. Res. Lett., 33(24), 1–4, doi:10.1029/2006GL027714, 2006.

Dorf, M., Butz, A., Camy-Peyret, C., Chipperfield, M. P., Kritten, L. and Pfeilsticker, K.: Bromine in the tropical troposphere and stratosphere as derived from balloon-borne BrO observations, Atmos. Chem. Phys., 8(23), 7265–7271, doi:10.5194/acp-8-7265-2008, 2008.

Evans, M. J., Jacob, D. J., Atlas, E., Cantrell, C. A., Eisele, F., Flocke, F., Fried, A., Mauldin, R. L., Ridley, B. A., Wert, B., Talbot, R., Blake, D., Heikes, B., Snow, J., Walega, J., Weinheimer, A. J. and Dibb, J.: Coupled evolution of BrO_x-ClO_x-HO_x-NO_x chemistry during bromine-catalyzed ozone depletion events in the arctic boundary layer, J. Geophys. Res., 108(D4), 8368, doi:10.1029/2002JD002732, 2003.

Fernandez, R. P., Salawitch, R. J., Kinnison, D. E., Lamarque, J.-F. and Saiz-Lopez, A.: Bromine partitioning in the tropical tropopause layer: implications for stratospheric injection, Atmos. Chem. Phys., 14(24), 13391–13410, doi:10.5194/acp-14-13391-2014, 2014.

Froyd, K. D., Murphy, D. M., Lawson, P., Baumgardner, D. and Herman, R. L.: Aerosols that form subvisible cirrus at the tropical tropopause, Atmos. Chem. Phys., 10(1), 209–218, doi:10.5194/acp-10-209-2010, 2010.

Gerbig, C., Schmitgen, S., Kley, D., Volz-Thomas, A., Dewey, K. and Haaks, D.: An improved fast-response vacuum-UV resonance fluorescence CO instrument, J. Geophys. Res. Atmos., 104(D1), 1699–1704, doi:10.1029/1998JD100031, 1999.

von Glasow, R., von Kuhlmann, R., Lawrence, M. G., Platt, U. and Crutzen, P. J.: Impact of reactive bromine chemistry in the troposphere, Atmos. Chem. Phys., 4(11/12), 2481–2497, doi:10.5194/acp-4-2481-2004, 2004.

Goodsite, M. E., Plane, J. M. C. and Skov, H.: A Theoretical Study of the Oxidation of Hg^0 to $HgBr_2$ in the Troposphere, , doi:10.1021/ES034680S, 2004.

Grainger, J. F. and Ring, J.: Anomalous Fraunhofer Line Profiles, Nature, 193(4817), 762–762, doi:10.1038/193762a0, 1962.

Harris, N. R. P., Carpenter, L. J., Lee, J. D., Vaughan, G., Filus, M. T., Jones, R. L., OuYang, B., Pyle, J. A., Robinson, A. D., Andrews, S. J., Lewis, A. C., Minaeian, J., Vaughan, A., Dorsey, J. R., Gallagher, M. W., Le Breton, M., Newton, R., Percival, C. J., Ricketts, H. M. A., Bauguitte, S. J.-B., Nott, G. J., Wellpott, A., Ashfold, M. J., Flemming, J., Butler, R., Palmer, P. I., Kaye, P. H., Stopford, C., Chemel, C., Boesch, H., Humpage, N., Vick, A., MacKenzie, A. R., Hyde, R., Angelov, P., Meneguz, E. and Manning, A. J.: Coordinated Airborne Studies in the Tropics (CAST), Bull. Am. Meteorol. Soc., 98(1), 145–162, doi:10.1175/BAMS-D-14-00290.1, 2017.

Holmes, C. D., Jacob, D. J. and Yang, X.: Global lifetime of elemental mercury against oxidation by atomic bromine in the free troposphere, Geophys. Res. Lett., 33(20), L20808, doi:10.1029/2006GL027176, 2006.

Hoskins, B. J.: Towards a PV- θ view of the general circulation, Tellus B, 43(4), doi:10.3402/tellusb.v43i4.15396, 1991.

Jensen, E. J., Pfister, L., Jordan, D. E., Bui, T. V., Ueyama, R., Singh, H. B., Lawson, P., Thornberry, T., Diskin, G., McGill, M., Pittman, J., Atlas, E. and Kim, J.: The NASA Airborne Tropical TRopopause EXperiment (ATTREX):High-Altitude Aircraft Measurements in the Tropical Western Pacific, [online] Available from: https://ntrs.nasa.gov/search.jsp?R=20160004203 (Accessed 15 March 2017), 2016.

Kley, D., Crutzen, P. J., Smit, H. G. J., Vömel, H., Oltmans, S. J., Grassl, H. and Ramanathan, V.: Observations of Near-Zero Ozone Concentrations Over the Convective Pacific: Effects on Air Chemistry, Science (80-.)., 274(5285) [online] Available from: http://science.sciencemag.org/content/274/5285/230 (Accessed 27 June 2017), 1996.

Ko, M. K. W. and Poulet, G. (Lead Authors), Blake, D. R., Boucher, O., Burkholder, J. H., Chin, M., Cox, R. A., George, C., Graf, H.-F., Holton, J. R., Jacob, D. J., Law, K. S., Lawrence, M. G., Midgley, P. M., Seakins, P. W., Shallcross, D. E., Strahan, S. E., Wuebbles, D. J. and Yokouchi, Y.: Surface ultraviolet radiation: Past and future, Chapter 5 in Scientific Assessment of Ozone Depletion: 2002, Global Ozone Research and Monitoring Project—Report No. 47, World Meteorological Organization, Geneva, Switzerland, 2003.

Kreycy, S., Camy-Peyret, C., Chipperfield, M. P., Dorf, M., Feng, W., Hossaini, R., Kritten, L., Werner, B. and Pfeilsticker, K.: Atmospheric test of the $J(BrONO_2)/k_{BrO+NO2}$ ratio: implications for total stratospheric Br_y and bromine-mediated ozone loss, Atmos. Chem. Phys., 13(13), 6263–6274, doi:10.5194/acp-13-6263-2013, 2013.

Lamarque, J.-F., Emmons, L. K., Hess, P. G., Kinnison, D. E., Tilmes, S., Vitt, F., Heald, C. L., Holland, E. A., Lauritzen, P. H., Neu, J., Orlando, J. J., Rasch, P. J. and Tyndall, G. K.: CAM-chem: description and evaluation of interactive atmospheric chemistry in the Community Earth System Model, Geosci. Model Dev., 5(2), 369–411, doi:10.5194/gmd-5-369-2012, 2012.

Lance, S., Brock, C. A., Rogers, D. and Gordon, J. A.: Water droplet calibration of the Cloud Droplet Probe (CDP) and in-flight performance in liquid, ice and mixed-phase clouds during ARCPAC, Atmos. Meas. Tech, 3(6), 1683–1706, doi:10.5194/amt-3-1683-2010, 2010.

Langford, A. O., Schofield, R., Daniel, J. S., Portmann, R. W., Melamed, M. L., Miller, H. L., Dutton, E. G. and Solomon, S.: On the variability of the Ring effect in the near ultraviolet: understanding the role of aerosols and multiple scattering, Atmos.

Chem. Phys. Atmos. Chem. Phys., 7, 575–586 [online] Available from: www.atmos-chem-phys.net/7/575/2007/ (Accessed 27 October 2016), 2007.

Lary, D. J.: Halogens and the chemistry of the free troposphere, Atmos. Chem. Phys., 5(1), 227–237, doi:10.5194/acp-5-227-2005, 2005.

Lelieveld, J., Crutzen, P. J. and Dentener, F. J.: Changing concentration, lifetime and climate forcing of atmospheric methane, Tellus B Chem. Phys. Meteorol., 50(2), 128–150, doi:10.1034/j.1600-0889.1998.t01-1-00002.x, 1998.

Liang, Q., Stolarski, R. S., Kawa, S. R., Nielsen, J. E., Douglass, A. R., Rodriguez, J. M., Blake, D. R., Atlas, E. L. and Ott, L. E.: Finding the missing stratospheric Br_y: a global modeling study of $CHBr_3$ and CH_2Br_2, Atmos. Chem. Phys., 10(5), 2269–2286, doi:10.5194/acp-10-2269-2010, 2010.

Lin, S.-J.: A “Vertically Lagrangian” Finite-Volume Dynamical Core for Global Models, Mon. Weather Rev., 132(10), 2293–2307, doi:10.1175/1520-0493(2004)132<2293:AVLFDC>2.0.CO;2, 2004.

Long, M. S., Keene, W. C., Easter, R. C., Sander, R., Liu, X., Kerkweg, A. and Erickson, D.: Sensitivity of tropospheric chemical composition to halogen-radical chemistry using a fully coupled size-resolved multiphase chemistry–global climate system: halogen distributions, aerosol composition, and sensitivity of climate-relevant gases, Atmos. Chem. Phys., 14(7), 3397–3425, doi:10.5194/acp-14-3397-2014, 2014.

Mahajan, A. S., Gómez Martín, J. C., Hay, T. D., Royer, S.-J., Yvon-Lewis, S., Liu, Y., Hu, L., Prados-Roman, C., Ordóñez, C., Plane, J. M. C. and Saiz-Lopez, A.: Latitudinal distribution of reactive iodine in the Eastern Pacific and its link to open ocean sources, Atmos. Chem. Phys., 12(23), 11609–11617, doi:10.5194/acp-12-11609-2012, 2012.

Meller, R. and Moortgat, G. K.: Temperature dependence of the absorption cross sections of formaldehyde between 223 and 323 K in the wavelength range 225-375 nm, J. Geophys. Res. Atmos., 105(D6), 7089–7101, doi:10.1029/1999JD901074, 2000.

Millán, L., Livesey, N., Read, W., Froidevaux, L., Kinnison, D., Harwood, R., MacKenzie, I. A. and Chipperfield, M. P.: New Aura Microwave Limb Sounder observations of BrO and implications for Br_y, Atmos. Meas. Tech, 5, 1741–1751, doi:10.5194/amt-5-1741-2012, 2012.

Molod, A., Takacs, L., Suarez, M. and Bacmeister, J.: Development of the GEOS-5 atmospheric general circulation model: evolution from MERRA to MERRA2, Geosci. Model Dev., 8(5), 1339–1356, doi:10.5194/gmd-8-1339-2015, 2015.

Murphy, D. M. and Thomson, D. S.: Halogen ions and NO+ in the mass spectra of aerosols in the upper troposphere and lower stratosphere, Geophys. Res. Lett., 27(19), 3217–3220, doi:10.1029/1999GL011267, 2000.

Murphy, D. M., Hudson, P. K., Thomson, D. S., Sheridan, P. J. and Wilson, J. C.: Observations of Mercury-Containing Aerosols, Environ. Sci. Technol., 40(10), 3163–3167, doi:10.1021/es052385x, 2006.

Navarro, M. A., Atlas, E. L., Saiz-Lopez, A., Rodriguez-Lloveras, X., Kinnison, D. E., Lamarque, J.-F., Tilmes, S., Filus, M., Harris, N. R. P., Meneguz, E., Ashfold, M. J., Manning, A. J., Cuevas, C. A., Schauffler, S. M. and Donets, V.: Airborne measurements of organic bromine compounds in the Pacific tropical tropopause layer., Proc. Natl. Acad. Sci. U. S. A., 112(45), 13789–13793, doi:10.1073/pnas.1511463112, 2015.

Neale, R. B., Richter, J., Park, S., Lauritzen, P. H., Vavrus, S. J., Rasch, P. J. and Zhang, M.: The Mean Climate of the Community Atmosphere Model (CAM4) in Forced SST and Fully Coupled Experiments, J. Clim., 26(14), 5150–5168, doi:10.1175/JCLI-D-12-00236.1, 2013.

Neuman, J. A., Nowak, J. B., Huey, L. G., Burkholder, J. B., Dibb, J. E., Holloway, J. S., Liao, J., Peischl, J., Roberts, J. M., Ryerson, T. B., Scheuer, E., Stark, H., Stickel, R. E., Tanner, D. J. and Weinheimer, A.: Bromine measurements in ozone depleted air over the Arctic Ocean, Atmos. Chem. Phys., 10(14), 6503–6514, doi:10.5194/acp-10-6503-2010, 2010.

Oetjen, H., Baidar, S., Krotkov, N. A., Lamsal, L. N., Lechner, M. and Volkamer, R.: Airborne MAX-DOAS measurements over California: Testing the NASA OMI tropospheric NO_2 product, J. Geophys. Res. Atmos., 118(13), 7400–7413, doi:10.1002/jgrd.50550, 2013.

Ordóñez, C., Lamarque, J.-F., Tilmes, S., Kinnison, D. E., Atlas, E. L., Blake, D. R., Sousa Santos, G., Brasseur, G. and Saiz-Lopez, A.: Bromine and iodine chemistry in a global chemistry-climate model: description and evaluation of very short-lived oceanic sources, Atmos. Chem. Phys., 12(3), 1423–1447, doi:10.5194/acp-12-1423-2012, 2012.

Pan, L. L., Paulik, L. C., Honomichl, S. B., Munchak, L. A., Bian, J., Selkirk, H. B. and V?mel, H.: Identification of the tropical tropopause transition layer using the ozone-water vapor relationship, J. Geophys. Res. Atmos., 119(6), 3586–3599, doi:10.1002/2013JD020558, 2014.

Pan, L. L., Atlas, E. L., Salawitch, R. J., Honomichl, S. B., Bresch, J. F., Randel, W. J., Apel, E. C., Hornbrook, R. S., Weinheimer, A. J., Anderson, D. C., Andrews, S. J., Baidar, S., Beaton, S. P., Campos, T. L., Carpenter, L. J., Chen, D., Dix, B., Donets, V., Hall, S. R., Hanisco, T. F., Homeyer, C. R., Huey, L. G., Jensen, J. B., Kaser, L., Kinnison, D. E., Koenig, T. K., Lamarque, J.-F. J.-F., Liu, C., Luo, J., Luo, Z. J., Montzka, D. D., Nicely, J. M., Pierce, R. B., Riemer, D. D., Robinson, T., Romashkin, P., Saiz-Lopez, A., Schauffler, S., Shieh, O., Stell, M. H., Ullmann, K., Vaughan, G., Volkamer, R. and Wolfe, G.: The Convective Transport of Active Species in the Tropics (CONTRAST) Experiment, Bull. Am. Meteorol. Soc., 98(1), doi:10.1175/BAMS-D-14-00272.1, 2017.

Parrella, J. P., Jacob, D. J., Liang, Q., Zhang, Y., Mickley, L. J., Miller, B., Evans, M. J., Yang, X., Pyle, J. A., Theys, N. and van Roozendael, M.: Tropospheric bromine chemistry: implications for present and pre-industrial ozone and mercury, Atmos. Chem. Phys., 12(15), 6723–6740, doi:10.5194/acp-12-6723-2012, 2012.

Pilewskie, P., Pommier, J., Bergstrom, R., Gore, W., Howard, S., Rabbette, M., Schmid, B., Hobbs, P. V. and Tsay, S. C.: Solar spectral radiative forcing during the Southern African Regional Science Initiative, J. Geophys. Res. Atmos., 108(D13), doi:10.1029/2002JD002411, 2003.

Platt, U. and Stutz, J.: Differential Optical Absorption Spectroscopy - Principles and Applications, Springer, Heidelberg., 2008.

Pundt, I., Pommereau, J. - P., Chipperfield, M. P., van Roozendael, M. and Goutail, F.: Climatology of the stratospheric BrO vertical distribution by balloon-borne UV–visible spectrometry, J. Geophys. Res., 107(D24), 4806, doi:10.1029/2002JD002230, 2002.

Read, K. A., Mahajan, A. S., Carpenter, L. J., Evans, M. J., Faria, B. V. E., Heard, D. E., Hopkins, J. R., Lee, J. D., Moller, S. J., Lewis, A. C., Mendes, L., McQuaid, J. B., Oetjen, H., Saiz-Lopez, A., Pilling, M. J. and Plane, J. M. C.: Extensive halogen-mediated ozone destruction over the tropical Atlantic Ocean, Nature, 453(7199), 1232–1235, doi:10.1038/nature07035, 2008.

Richter, A., Wittrock, F., Ladstätter-Weißenmayer, A. and Burrows, J. P.: GOME measurements of stratospheric and tropospheric BrO, Adv. Sp. Res., 29(11), 1667–1672, doi:10.1016/S0273-1177(02)00123-0, 2002.

Saiz-Lopez, A. and Fernandez, R. P.: On the formation of tropical rings of atomic halogens: Causes and implications, Geophys. Res. Lett., 43(6), 2928–2935, doi:10.1002/2015GL067608, 2016.

Saiz-Lopez, A. and von Glasow, R.: Reactive halogen chemistry in the troposphere, Chem. Soc. Rev., 41(19), 6448–6472, doi:10.1039/c2cs35208g, 2012.

Saiz-Lopez, A., Lamarque, J.-F. J.-F., Kinnison, D. E., Tilmes, S., Ordóñez, C., Orlando, J. J., Conley, A. J., Plane, J. M. C., Mahajan, A. S., Sousa Santos, G., Atlas, E. L., Blake, D. R., Sander, S. P., Schauffler, S., Thompson, A. M. and Brasseur, G.: Estimating the climate significance of halogen-driven ozone loss in the tropical marine troposphere, Atmos. Chem. Phys., 12(9), 3939–3949, doi:10.5194/acp-12-3939-2012, 2012.

Saiz-Lopez, A., Fernandez, R. P., Ordóñez, C., Kinnison, D. E., Gómez Martín, J. C., Lamarque, J.-F. and Tilmes, S.: Iodine chemistry in the troposphere and its effect on ozone, Atmos. Chem. Phys., 14(23), 13119–13143, doi:10.5194/acp-14-13119-2014, 2014.

Saiz-Lopez, A., Baidar, S., Cuevas, C. A., Koenig, T. K., Fernandez, R. P., Dix, B., Kinnison, D. E., Lamarque, J.-F., Rodriguez-Lloveras, X., Campos, T. L. and Volkamer, R.: Injection of iodine to the stratosphere, Geophys. Res. Lett., 42(16), 6852–6859, doi:10.1002/2015GL064796, 2015.

Salawitch, R. J., Weisenstein, D. K., Kovalenko, L. J., Sioris, C. E., Wennberg, P. O., Chance, K., Ko, M. K. W. and McLinden, C. A.: Sensitivity of ozone to bromine in the lower stratosphere, Geophys. Res. Lett., 32(5), L05811, doi:10.1029/2004GL021504, 2005.

Sander, S. P., Friedl, R. R., Abbatt, J. P. D., Barker, J. R., Burkholder, J. B., Golden, D. M., Kold, C. E., Kuylo, M. J., Moortgat, G. K., Wine, P. H., Huie, R. E. and Orkin, V. L.: Chemical Kinetics and Photochemical Data for Use in Atmospheric Studies, Evaluation No. 17, Pasadena. [online] Available from: http://jpldataeval.jpl.nasa.gov (Accessed 25 October 2016), 2011.

Schauffler, S. M., Atlas, E. L., Blake, D. R., Flocke, F., Lueb, R. A., Lee-Taylor, J. M., Stroud, V. and Travnicek, W.: Distributions of brominated organic compounds in the troposphere and lower stratosphere, J. Geophys. Res. Atmos., 104(D17), 21513–21535, doi:10.1029/1999JD900197, 1999.

Schmidt, J. A., Jacob, D. J., Horowitz, H. M., Hu, L., Sherwen, T., Evans, M. J., Liang, Q., Suleiman, R. M., Oram, D. E., Le Breton, M., Percival, C. J., Wang, S., Dix, B. and Volkamer, R.: Modeling the observed tropospheric BrO background: Importance of multiphase chemistry and implications for ozone, OH, and mercury, J. Geophys. Res. Atmos., 121(19), 11,819-11,835, doi:10.1002/2015JD024229, 2016.

Serdyuchenko, A., Gorshelev, V., Weber, M., Chehade, W. and Burrows, J. P.: High spectral resolution ozone absorption cross-sections – Part 2: Temperature dependence, Atmos. Meas. Tech, 7, 625–636, doi:10.5194/amt-7-625-2014, 2014.

Sherwen, T., Schmidt, J. A., Evans, M. J., Carpenter, L. J., Großmann, K., Eastham, S. D., Jacob, D. J., Dix, B., Koenig, T. K., Sinreich, R., Ortega, I., Volkamer, R., Saiz-Lopez, A., Prados-Roman, C., Mahajan, A. S. and Ordóñez, C.: Global impacts of tropospheric halogens (Cl, Br, I) on oxidants and composition in GEOS-Chem, Atmos. Chem. Phys., 16(18), 12239–12271, doi:10.5194/acp-16-12239-2016, 2016.

Sherwen, T., Evans, M. J., Sommariva, R., Hollis, L. D. J., Ball, S. M., Monks, P. S., Reed, C., Carpenter, L. J., Lee, J. D., Forster, G., Bandy, B., Reeves, C. E., Bloss, W. J., Monks, P. S., Oetjen, H., Plane, J. M. C., Whitehead, J. D., Sander, R., Hall, S. R., Ullmann, K., Sharp, T., Stone, D., Heard, D. E., Fleming, Z. L., Leigh, R., Shallcross, D. E., Percival, C. J., Orr-Ewing, A. J., Plane, J. M. C., Potin, P., Shillings, A. J. L., Thomas, F., Glasow, R. von, Wada, R., Whalley, L. K. and Whitehead, J. D.: Effects of halogens on European air-quality, Faraday Discuss., 16, 11433–11450, doi:10.1039/C7FD00026J, 2017a.

Sherwen, T., Evans, M. J., Carpenter, L. J., Schmidt, J. A. and Mickley, L. J.: Halogen chemistry reduces tropospheric O_3 radiative forcing, Atmos. Chem. Phys., 17(2), 1557–1569, doi:10.5194/acp-17-1557-2017, 2017b.

Shetter, R. E. and Müller, M.: Photolysis frequency measurements using actinic flux spectroradiometry during the PEM-Tropics mission: Instrumentation description and some results, J. Geophys. Res. Atmos., 104(D5), 5647–5661, doi:10.1029/98JD01381, 1999.

Simpson, W. R., Brown, S. S., Saiz-Lopez, A., Thornton, J. A. and von Glasow, R.: Tropospheric Halogen Chemistry: Sources, Cycling, and Impacts, Chem. Rev., 115(10), 4035–4062, doi:10.1021/cr5006638, 2015.

Sinnhuber, B.-M., Sheode, N., Sinnhuber, M., Chipperfield, M. P. and Feng, W.: The contribution of anthropogenic bromine emissions to past stratospheric ozone trends: a modelling study, Atmos. Chem. Phys., 9(8), 2863–2871, doi:10.5194/acp-9-2863-2009, 2009.

Spinei, E., Cede, A., Herman, J., Mount, G. H., Eloranta, E., Morley, B., Baidar, S., Dix, B., Ortega, I., Koenig, T. and Volkamer, R.: Ground-based direct-sun DOAS and airborne MAX-DOAS measurements of the collision-induced oxygen complex, O_2O_2, absorption with significant pressure and temperature differences, Atmos. Meas. Tech., 8(2), 793–809, doi:10.5194/amt-8-793-2015, 2015.

Stachnik, R. A., Millán, L., Jarnot, R., Monroe, R., McLinden, C., Kühl, S., Puķīte, J., Shiotani, M., Suzuki, M., Kasai, Y., Goutail, F., Pommereau, J. P., Dorf, M. and Pfeilsticker, K.: Stratospheric BrO abundance measured by a balloon-borne submillimeterwave radiometer, Atmos. Chem. Phys., 13(6), 3307–3319, doi:10.5194/acp-13-3307-2013, 2013.

Stutz, J., Werner, B., Spolaor, M., Scalone, L., Festa, J., Tsai, C., Cheung, R., Colosimo, S. F., Tricoli, U., Raecke, R., Hossaini, R., Chipperfield, M. P., Feng, W., Gao, R.-S., Hintsa, E. J., Elkins, J. W., Moore, F. L., Daube, B., Pittman, J., Wofsy, S. and Pfeilsticker, K.: A new Differential Optical Absorption Spectroscopy instrument to study atmospheric chemistry from a high-altitude unmanned aircraft, Atmos. Meas. Tech., 10(3), 1017–1042, doi:10.5194/amt-10-1017-2017, 2017.

Thalman, R. and Volkamer, R.: Temperature dependent absorption cross-sections of O_2-O_2 collision pairs between 340 and 630 nm and at atmospherically relevant pressure, Phys. Chem. Chem. Phys., 15(37), 15371–81, doi:10.1039/c3cp50968k, 2013.

Thalman, R., Zarzana, K. J., Tolbert, M. A. and Volkamer, R.: Rayleigh scattering cross-section measurements of nitrogen, argon, oxygen and air, J. Quant. Spectrosc. Radiat. Transf., 147, 171–177, doi:10.1016/j.jqsrt.2014.05.030, 2014.

Theys, N., Van Roozendael, M., Hendrick, F., Fayt, C., Hermans, C., Baray, J.-L., Goutail, F., Pommereau, J.-P. and De Mazière, M.: Retrieval of stratospheric and tropospheric BrO columns from multi-axis DOAS measurements at Reunion Island (21° S, 56° E), Atmos. Chem. Phys., 7(18), 4733–4749, doi:10.5194/acp-7-4733-2007, 2007.

Theys, N., Van Roozendael, M., Hendrick, F., Yang, X., De Smedt, I., Richter, A., Begoin, M., Errera, Q., Johnston, P. V., Kreher, K. and De Mazière, M.: Global observations of tropospheric BrO columns using GOME-2 satellite data, Atmos. Chem. Phys., 11(4), 1791–1811, doi:10.5194/acp-11-1791-2011, 2011.

Vandaele, A. C., Hermans, C., Simon, P. C., Carleer, M., Colin, R., Fally, S., Mérienne, M. F., Jenouvrier, A. and Coquart, B.: Measurements of the NO_2 absorption cross-section from 42 000 cm^{-1} to 10 000 cm^{-1} (238–1000 nm) at 220 K and 294 K, J. Quant. Spectrosc. Radiat. Transf., 59(3–5), 171–184, doi:10.1016/S0022-4073(97)00168-4, 1998.

Volkamer, R., Baidar, S., Campos, T. L., Coburn, S., DiGangi, J. P., Dix, B., Eloranta, E. W., Koenig, T. K., Morley, B., Ortega, I., Pierce, B. R., Reeves, M., Sinreich, R., Wang, S., Zondlo, M. A. and Romashkin, P. A.: Aircraft measurements of BrO, IO, glyoxal, NO_2, H_2O, O_2–O_2 and aerosol extinction profiles in the tropics: comparison with aircraft-/ship-based in situ and lidar measurements, Atmos. Meas. Tech., 8(5), 2121–2148, doi:10.5194/amt-8-2121-2015, 2015.

Wagner, T., Leue, C., Wenig, M., Pfeilsticker, K. and Platt, U.: Spatial and temporal distribution of enhanced boundary layer BrO concentrations measured by the GOME instrument aboard ERS-2, J. Geophys. Res. Atmos., 106(D20), 24225–24235, doi:10.1029/2000JD000201, 2001.

Wang, S., Schmidt, J. A., Baidar, S., Coburn, S., Dix, B., Koenig, T. K., Apel, E., Bowdalo, D., Campos, T. L., Eloranta, E., Evans, M. J., DiGangi, J. P., Zondlo, M. A., Gao, R.-S., Haggerty, J. A., Hall, S. R., Hornbrook, R. S., Jacob, D., Morley, B., Pierce, B., Reeves, M., Romashkin, P., ter Schure, A. and Volkamer, R.: Active and widespread halogen chemistry in the tropical and subtropical free troposphere, Proc. Natl. Acad. Sci., 112(30), 9281–9286, doi:10.1073/pnas.1505142112, 2015.

Werner, B., Stutz, J., Spolaor, M., Scalone, L., Raecke, R., Festa, J., Colosimo, F., Cheung, R., Tsai, C., Hossaini, R., Chipperfield, M. P., Taverna, G. S., Feng, W., Elkins, J. W., Fahey, D. W., Gao, R.-S., Hintsa, E. J., Thornberry, T. D., Moore, F. L., Navarro, M. A., Atlas, E., Daube, B., Pittman, J., Wofsy, S. and Pfeilsticker, K.: Probing the subtropical lowermost stratosphere, tropical upper troposphere, and tropopause layer for inorganic bromine, Atmos. Chem. Phys., 1–43, doi:10.5194/acp-2016-656, 2017.

Wilmouth, D. M., Thomas F. Hanisco, Neil M. Donahue, A. and Anderson, J. G.: Fourier Transform Ultraviolet Spectroscopy of the A $^2\Pi_{3/2} \leftarrow$ X $^2\Pi_{3/2}$ Transition of BrO, , doi:10.1021/JP991651O, 1999.

Wofsy, S. C., McElroy, M. B. and Yung, Y. L.: The chemistry of atmospheric bromine, Geophys. Res. Lett., 2(6), 215–218, doi:10.1029/GL002i006p00215, 1975.

Yang, X., Cox, R. A., Warwick, N. J., Pyle, J. A., Carver, G. D., O'Connor, F. M. and Savage, N. H.: Tropospheric bromine chemistry and its impacts on ozone: A model study, J. Geophys. Res., 110(D23), D23311, doi:10.1029/2005JD006244, 2005.

Zondlo, M. A., Paige, M. E., Massick, S. M. and Silver, J. A.: Vertical cavity laser hygrometer for the National Science Foundation Gulfstream-V aircraft, J. Geophys. Res., 115(D20), D20309, doi:10.1029/2010JD014445, 2010.

Table 1: Instruments aboard the NSF GV research aircraft used to constrain the box-model.

Instrument	**Parameters used in this work**	**Time Resolution**
AMAX-DOAS	BrO, IO, NO_2	30 s
AWAS	Ethane, Propane, Isobutane, n-Butane, CFC-11, Benzene	minutes[a]
Chemiluminescence	NO, NO_2, O_3	1 s
HARP	Actinic flux (upward and downward) is used to calculate photolysis rates	1 s
ISAF	HCHO	1 s
PICARRO	Methane	1 s
TOGA	Propane, Isobutane, n-Butane, HCHO, CFC-11, Benzene	2.8 min
UHSAS	Aitken and accumulation mode aerosol surface area	1 s
Aerolaser VUV flourescence	CO	2 s
GV	Pressure, temperature, water, location	1 s

[a] AWAS samples were collected at intervals determined in flight by an operator

Table 2: DOAS fitting windows used in fitting BrO, O_4, and NO_2 in QDOAS.

Cross Section	Wavelength Window (nm)		
	BrO 335-359 nm[h]	O_4 350-387.5 nm[i]	NO_2 356–380 nm[j]
BrO[a]	✖	✖	✖
HCHO[b]	✖	✖	✖
NO_2[c]	✖	✖	✖
O_4[d]	✖	✖	✖
O_3[e]	✖	✖	✖
O_3 x λ[e]	✖	✖	✖
Ring[f]	✖	✖	✖
Ring x λ[f,g]	✖	✖	✖

[a] Wilmouth et al. (1999) at 228 K. [b] Meller and Moortgat (2000) at 298 K. [c] Vandaele et al. (1998) at 220 K. [d] Thalman and Volkamer (2013) at 296 K. The O_4 in the BrO window was not fit, but rather constrained to the value obtained in the O_4 optimized fit and scaled to the wavelength of the O_4 peak at 350 nm. [e] Serdyuchenko et al. (2014) at 223 K and 243 K, the wavelength scaled O_3 uses the 223 K cross section. This and the 243 K cross section are orthogonlized to the 223 K cross section. [f] Ring was calculated using the QDOAS (Danckaert et al., 2012) tool using the reference spectrum for wavelength calibration. [g] This matches the treatment in Langford et al. (2007). [h] The BrO window used a polynomial of order 6 and a linear offset correction. O_3 and NO_2 were orthogonalized to the first 3 terms of the polynomial. [i] The O_4 window used a polynomial of order 5 and a linear offset correction. O_3 and NO_2 were orthogonalized to the first 3 terms of the polynomial. [j] The NO_2 window used a polynomial of order 5 and a linear offset correction.

Table 3: Box Model sensitivity studies probing the effects of aerosol surface area, ice, and kinetics for $BrONO_2$.

Box Model Case	**Surface Areas**	**Kinetics**
Case 0	UHSAS Measured Surface Area	JPL (Sander et al., 2011)
Case 1	UHSAS Measured Surface Area × 4[a]	JPL idem
Case 2	UHSAS Measured Surface Area × 4 and GEOS-Chem ice climatology	JPL idem
Case 3	UHSAS Measured Surface Area × 4 and GEOS-Chem ice climatology	Kreycy et al., 2013

[a] Based on results of optical closure study in Section 3.1 and Figure 3 of Volkamer et al., 2015.

Atmos. Chem. Phys. Discuss., https://doi.org/10.5194/acp-2017-572
Manuscript under review for journal Atmos. Chem. Phys.
Discussion started: 7 July 2017

Table 4: Summary of BrO and Br_y mixing ratios over the tWPO.

Altitude	BrO ppt[a]	Br_y ppt[b]				
		case 0	case 1	case 2	case 3	pooled
MBL, 0-0.5km	1.7 (1.0, 3.8)	13.8	13.8	13.8	13.8	13.8 (5.5, 30.2)
TL, 0.5-2.0 km	1.2 (0.6, 1.3)	5.8	5.8	5.8	5.8	5.8 (3.4, 8.7)
Lower FT, 2.0-6.5 km	0.7 (0.4, 0.9)	2.8	2.8	2.8	2.8	2.8 (1.6, 5.0)
Mid FT, 6.5-9.5 km	0.6 (0.5, 1.0)	3.6	1.6	1.6	1.6	2.1 (1.3, 3.6)
Upper FT, 9.5-12.5 km	0.6 (0.3, 0.7)	6.2	2.1	1.7	1.7	2.1 (1.6, 4.4)
Convective TTL[c]	0.9 (0.5, 1.1)	4.8	3.3	2.6	2.6	3.3 (2.6, 4.3)
Aged TTL[d]	1.2 (0.9, 1.8)	2.7	2.7	2.6	2.6	2.7 (2.0, 3.5)
LS[e]	3.1 (2.8, 3.2)	6.9	6.9	6.9	6.0	6.9 (6.5, 7.4)

[a]BrO is reported as follows: median, (1st quartile, 3rd quartile). [b]Br_y values are the medians for each of the chemical cases, the "pooled" values report the median, (1st quartile, 3rd quartile) for cases 0, 1 and 2. Air masses above 12.5 km are classified as follows: [c]Convective TTL $H_2O/O_3 > 0.1$ ppm/ppb, [d]Aged TTL $H_2O/O_3 < 0.1$ ppm/ppb, [e]LS $O_3 > 200$ ppt.

5

Table 5: Comparison of partial and total tropospheric BrO VCDs measured by AMAX-DOAS with different models. Values in parentheses indicate the 1st and 3rd quartile.

Altitude	**BrO VCD ×10^{12} (AMAX-DOAS measurements)**	**BrO VCD (GEOS-Chem no SSA source)**	**BrO VCD (GEOS-Chem w/ SSA source)**	**BrO VCD (CAM-chem)**
MBL	2.1 (1.2, 4.7)	1.0 (0.2, 1.5)	3.6 (0.5, 9.0)	0.2 (0.1, 0.6)
TL	4.0 (2.8, 7.3)	2.0 (0.8, 3.3)	6.1 (3.1, 10.6)	0.4 (0.2, 1.3)
Lower FT	5.7 (2.9, 6.8)	2.1 (1.2, 4.1)	4.5 (2.4, 8.0)	1.4 (0.7, 2.2)
Mid FT	2.2 (1.4, 3.2)	2.7 (1.7, 3.8)	4.6 (3.3, 5.9)	1.1 (0.7, 1.6)
Upper FT	1.3 (0.7, 1.7)	0.8 (0.4, 1.6)	1.2 (0.6, 2.2)	0.5 (0.3, 0.9)
TTL	1.1 (0.8, 1.5)	0.6 (0.2, 1.4)	0.7 (0.2, 1.7)	0.5 (0.3, 1.0)
Troposphere	16.5 (9.6, 25.2)	9.1 (4.5, 15.8)	20.7 (10.1, 37.4)	4.1 (2.4, 7.6)

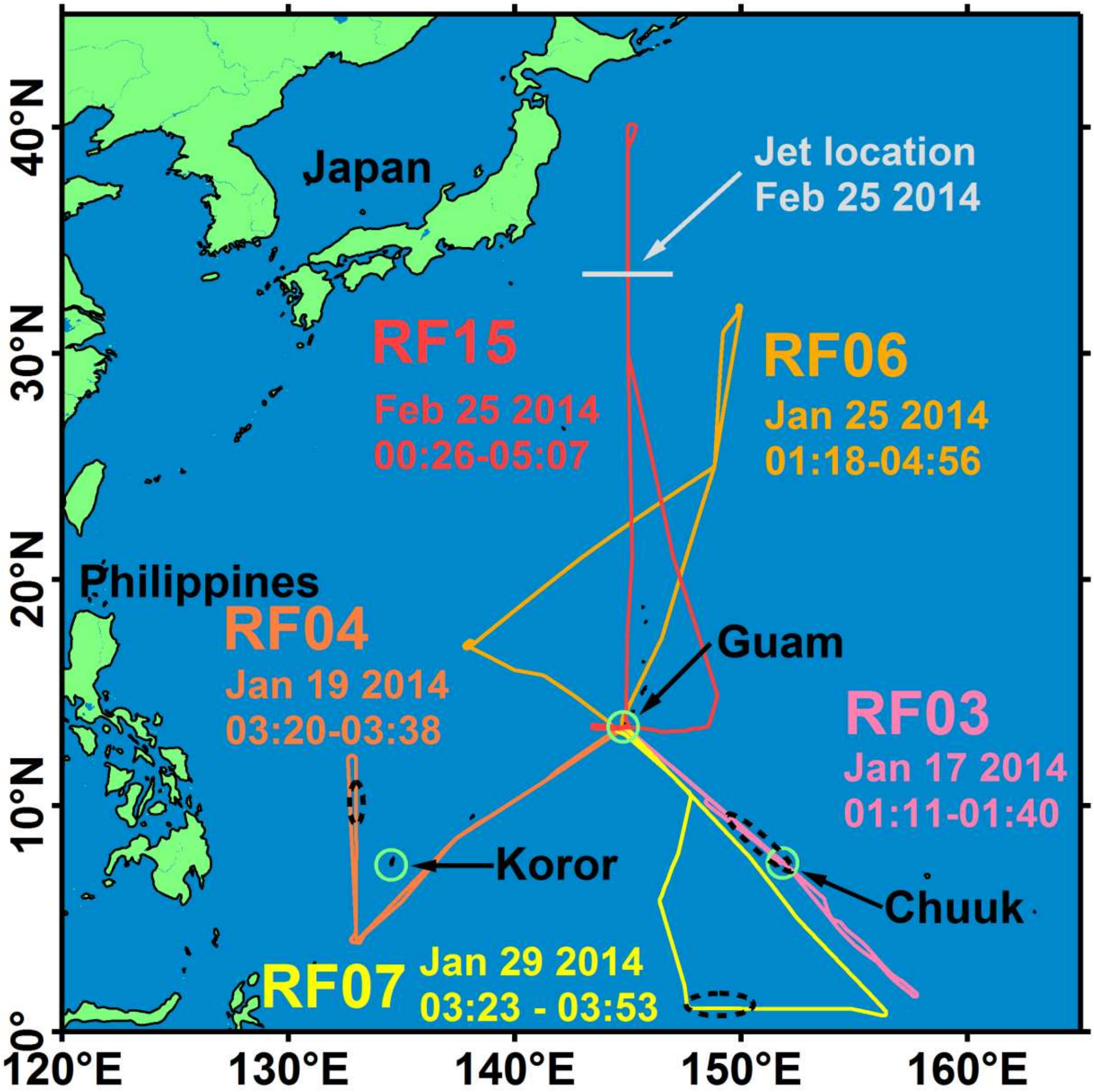

Figure 1: Flight tracks with the locations of profile case studies (0-15 km) used in this work. For northbound flights RF06 and RF15, the times reflect periods used for detailed modeling. For RF03, RF04, and RF07, the locations of the vertical profiles are indicated by the black dashed ellipses, and the times listed are those of the profiles, and low level flight legs in the boundary layer.

5

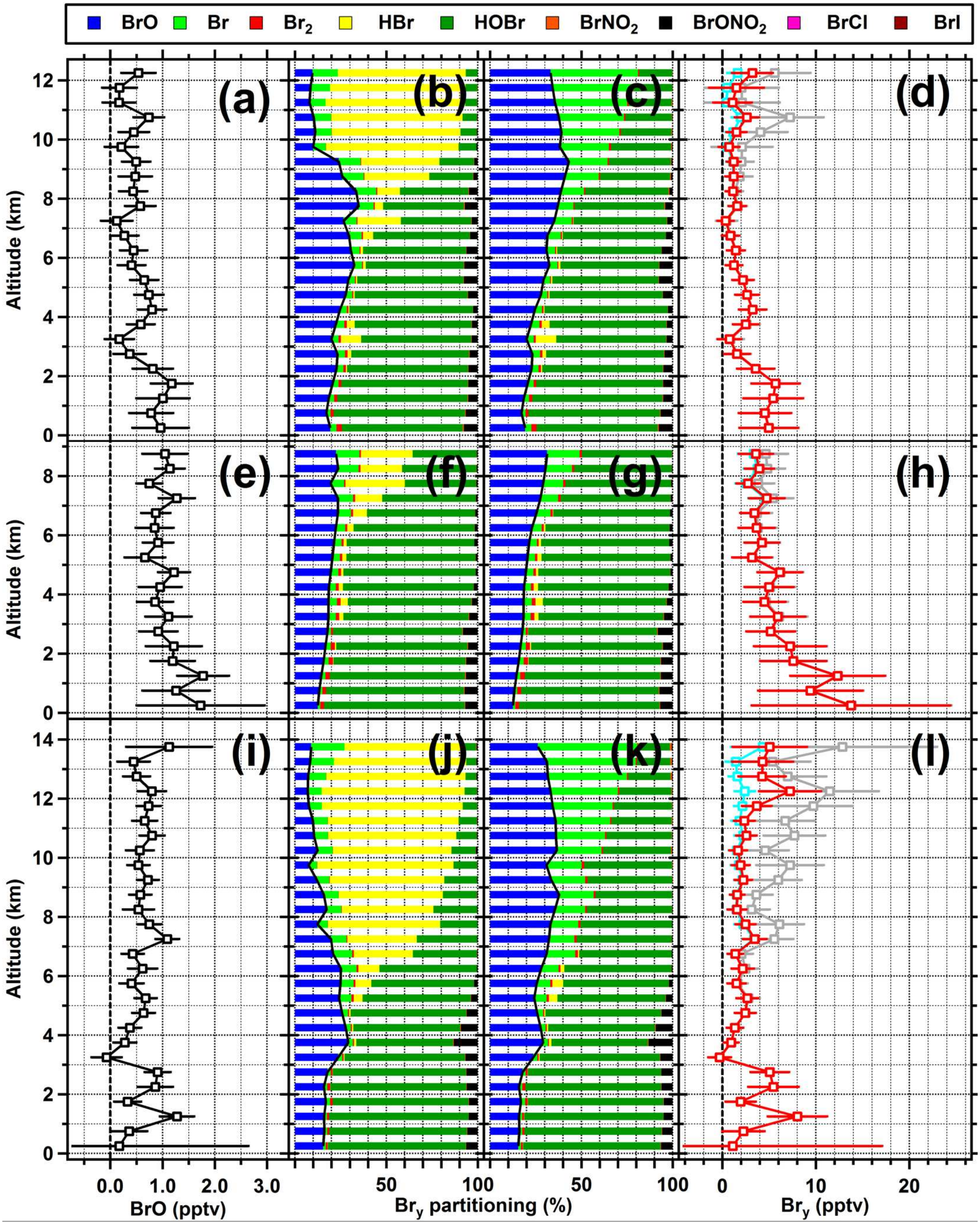
BrO
Br
Br_2
HBr
HOBr
$BrNO_2$
$BrONO_2$
BrCl
BrI
(a)
(b)
(c)
(d)
(e)
(f)
(g)
(h)
(i)
(j)
(k)
(l)
Altitude (km)
Altitude (km)
Altitude (km)
0
2
4
6
8
10
12
14
0.0
1.0
2.0
3.0
BrO (pptv)
50
100
50
100
Br_y partitioning (%)
0
10
20
Br_y (pptv)

Atmos. Chem. Phys. Discuss., https://doi.org/10.5194/acp-2017-572
Manuscript under review for journal Atmos. Chem. Phys.
Discussion started: 7 July 2017

Figure 2: BrO, Br_y, and Bry partitioning for RF03 (a-d), RF04 (e-h), RF07 (i-l). BrO mixing ratios were obtained by optimal estimation. Partitioning of Br_y species: (b, f, and j) case 0; (c, g, and k) case 2; (black line) BrO/Br_y ratio. (d, h, and l) Br_y from case 0 (grey); case 1(red); case 2 (cyan).

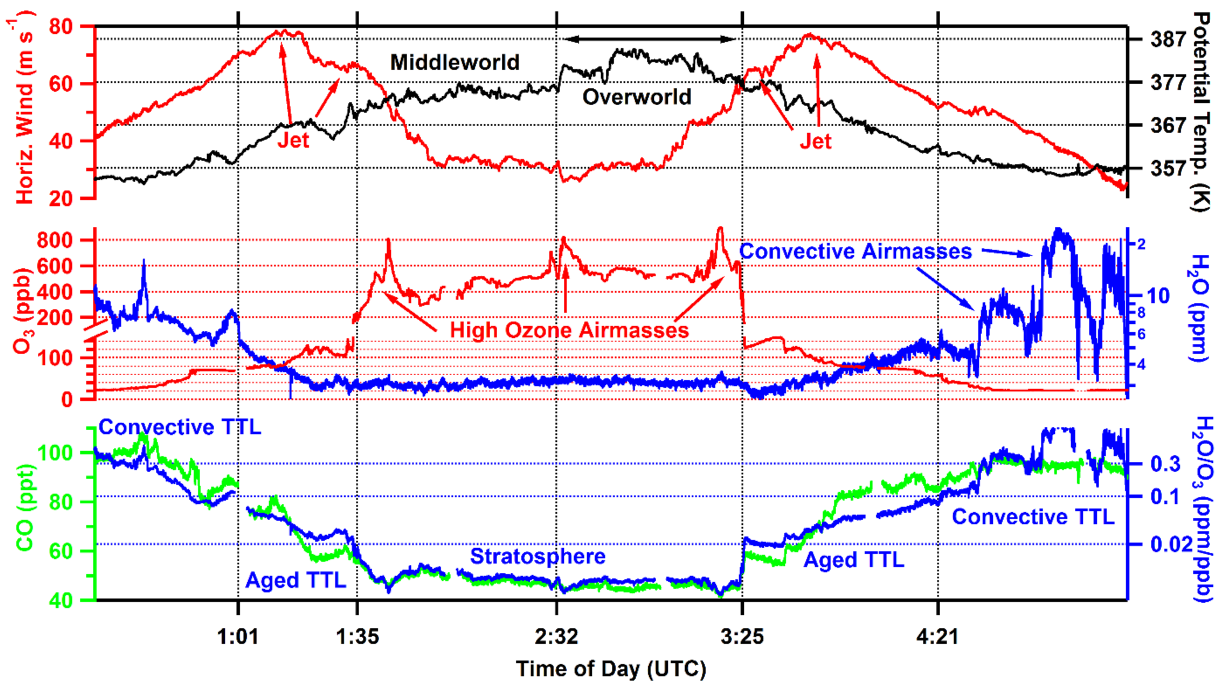

Figure 3: Meteorological and chemical tracers during RF15. Top panel: (red) horizontal windspeed; (black) potential temperature (θ). The subtropical jet stream is visible where the horizontal wind maxima have tropospheric and stratospheric halves (indicated by arrows). The black arrow indicates the overworld (here: θ above 377 K). Middle panel: (red) O_3; (blue) H_2O. The troposphere - stratosphere transition is marked at 200 ppb O_3. Positive departures in H_2O mark convective air masses. Bottom panel: (green) CO; (blue) H_2O/O_3 ratio. The 0.1 ppm/ppb line is used to separate the aged TTL from the convective TTL. The times marked indicate the transitions (from left to right) 1:01 convective TTL to aged TTL, 1:35 aged TTL to middleworld LS, 2:32 middleworld LS to overworld LS, 3:25 overworld LS to aged TTL, and 4:21 aged TTL to convective TTL.

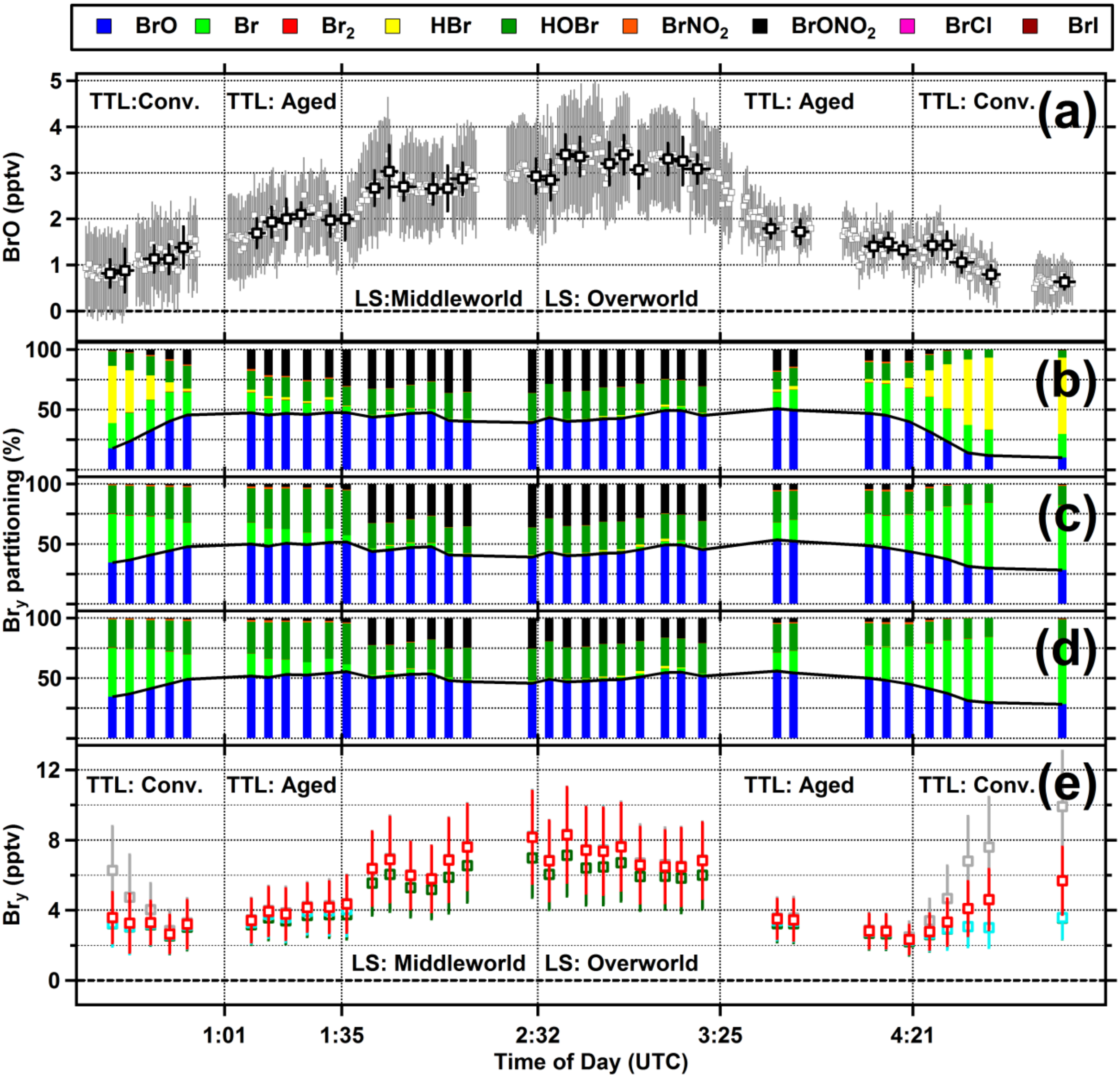

Figure 4: BrO, Br_y, and Br_y partitioning during the RF15 jet crossing flight. (a) (black) 5 min average BrO used for model input; (grey) 30 s data. (b-d) Partitioning of Br_y species from box model for (b) case 0, (c) case 2, (d) case 3; (black line) BrO/Br_y ratio. (e) Br_y inferred along the flight track using the measured BrO and the modeled ratio; (grey) case 0; (red) case 1; (cyan) case 2; (dark green) case 3.

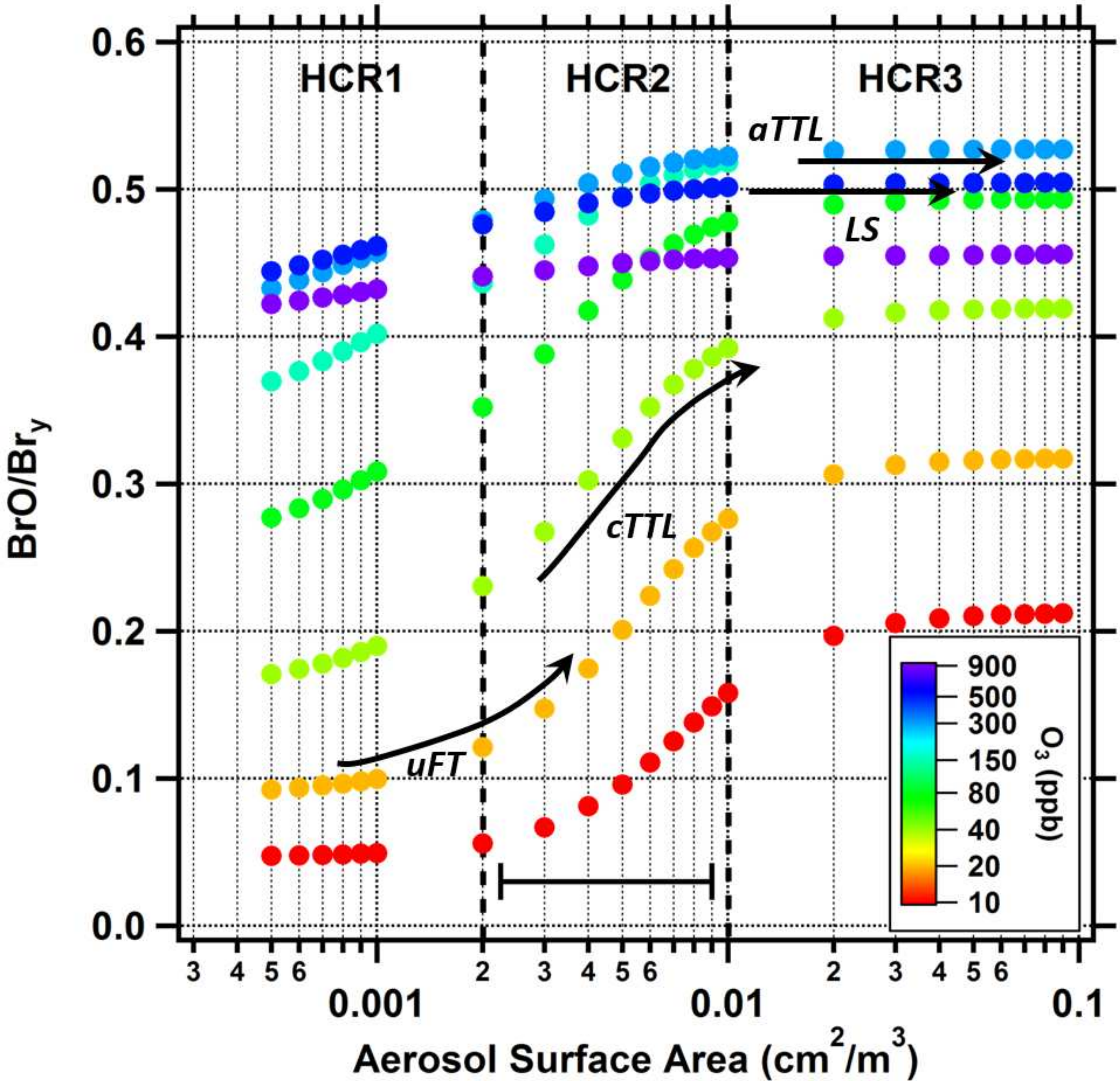

5 **Figure 5: Sensitivity of the BrO/Br$_y$ ratio surface area (to SA) and O$_3$ concentration. Conditions are representative of the upper troposphere. (dashed vertical lines) mark the heterogeneous chemical regimes (HCR, see Sect. 2.3.1). The horizontal bar at the bottom marks a factor of four in SA along the logarithmic abscissa (i.e., the difference between case 0 and case 1). Arrows mark the corresponding sensitivity of the BrO/Br$_y$ ratio in the upper FT (uFT), convective TTL (cTTL), aged TTL (aTTL), and LS. The largest sensitivity is observed in the upper FT and convective TTL, while the aged TTL and LS are insensitive.**

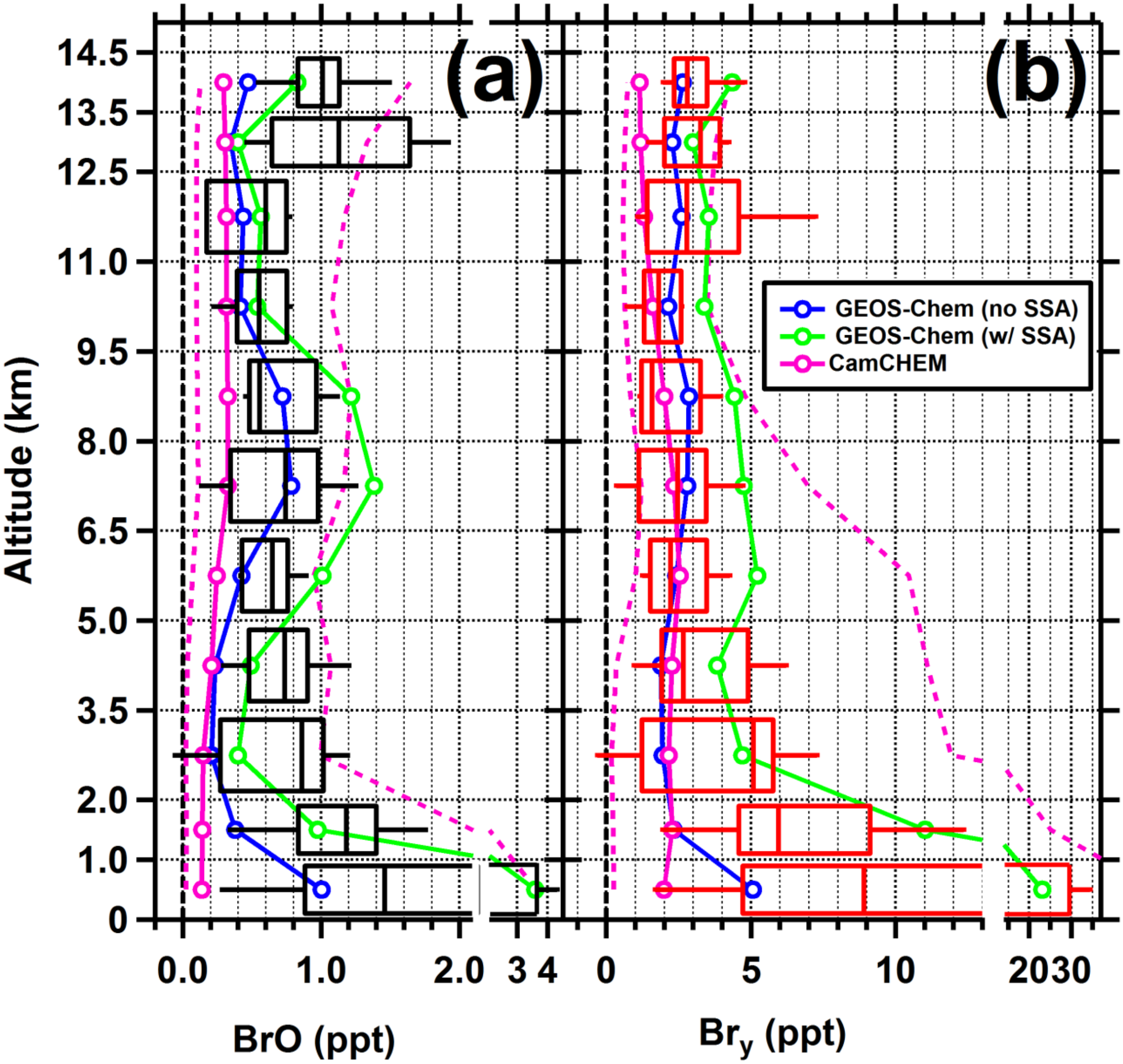

Figure 6: Vertical profile of BrO and Br_y over the tWPO and comparison with global models. Boxes and whiskers are for observations (black), and box model case 1 (red). Boxes indicate the 25th and 75th percentile, whiskers the 10th and 90th percentile. Stratospheric points (as classified in Sect. 3.2) are not included in the statistics for models or data. Lines indicate median global model profiles for the case studies, (blue) GEOS-Chem without a SSA bromine source, (green) GEOS-Chem with a heterogeneous SSA bromine source, (magenta) CAM-chem (includes SSA bromine source). The dashed magenta lines indicate the 5th and 95th percentile for CAM-chem.

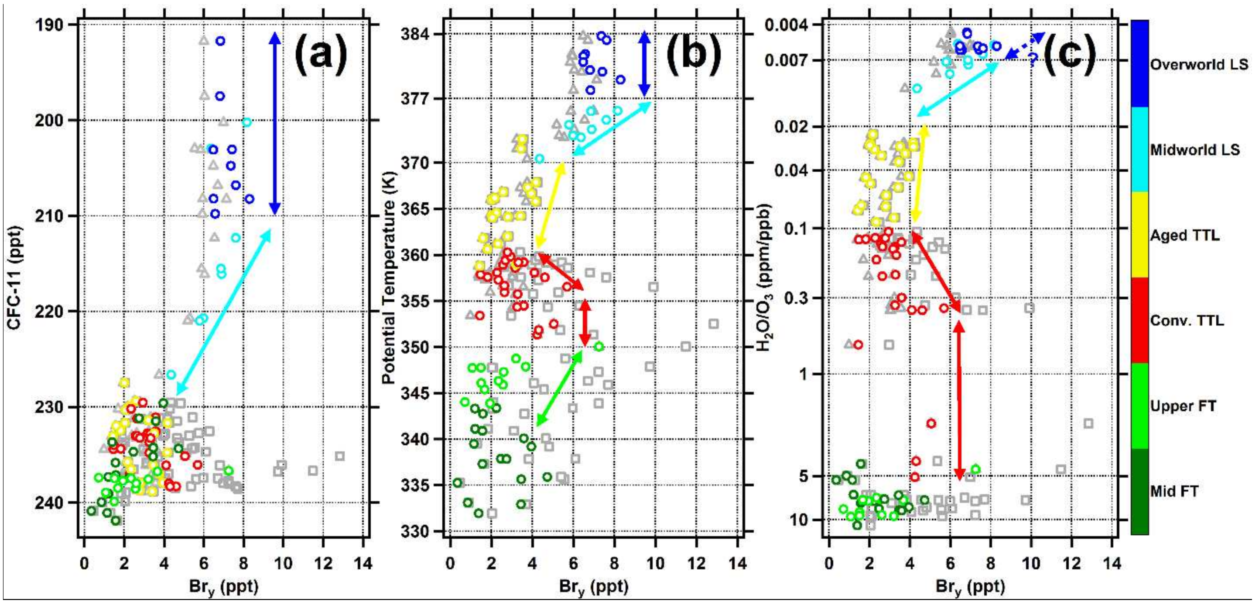

Figure 7: Br_y vertical structure in the UTLS. (colored circles) Br_y from box-model case 1; the color represents different air mass types. (grey squares) case 0; (grey triangles) case 3. Tracer correlations with (a) CFC-11, (b) potential temperature, and (c) H_2O/O_3 ratio have been constructed such that the top is more stratospheric, while the bottom is tropospheric.

Atmos. Chem. Phys. Discuss., https://doi.org/10.5194/acp-2017-572
Manuscript under review for journal Atmos. Chem. Phys.
Discussion started: 7 July 2017

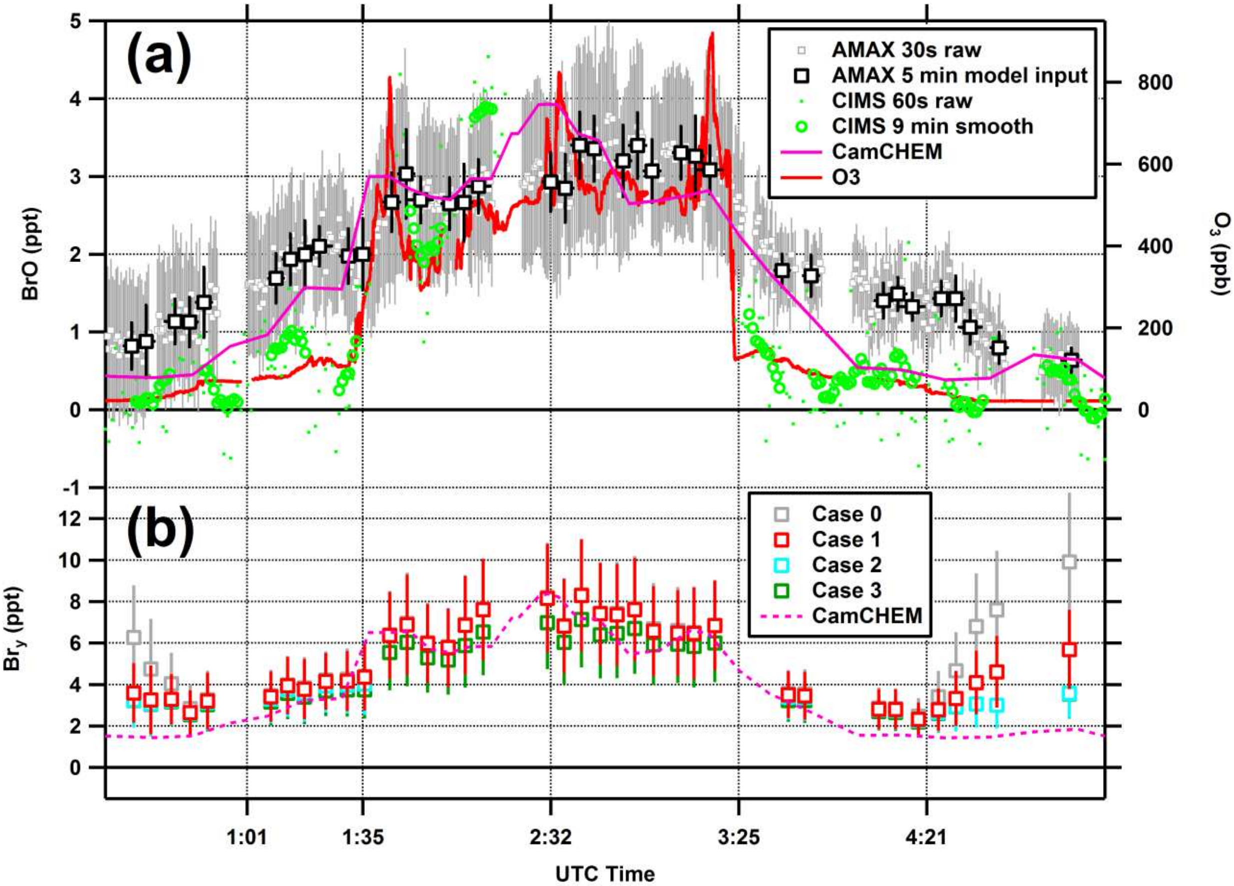

5 **Figure 8: Comparison of BrO and Br_y along the RF15 flight track with CAM-chem. (a) Raw output is shown for DOAS (grey) and GT CIMS BrO (green); along with the 5 minute averages for DOAS (black squares), and a moving 9 minute box average for GT CIMS (green circles); (blue line) CAM-chem predicted BrO; (red line) measured O_3 to indicate the entrance of the LS; GT CIMS data is screened for O_3 > 480 ppb. (b) Comparison of box model Br_y with CAM-chem.**

Atmos. Chem. Phys. Discuss., https://doi.org/10.5194/acp-2017-572
Manuscript under review for journal Atmos. Chem. Phys.
Discussion started: 7 July 2017

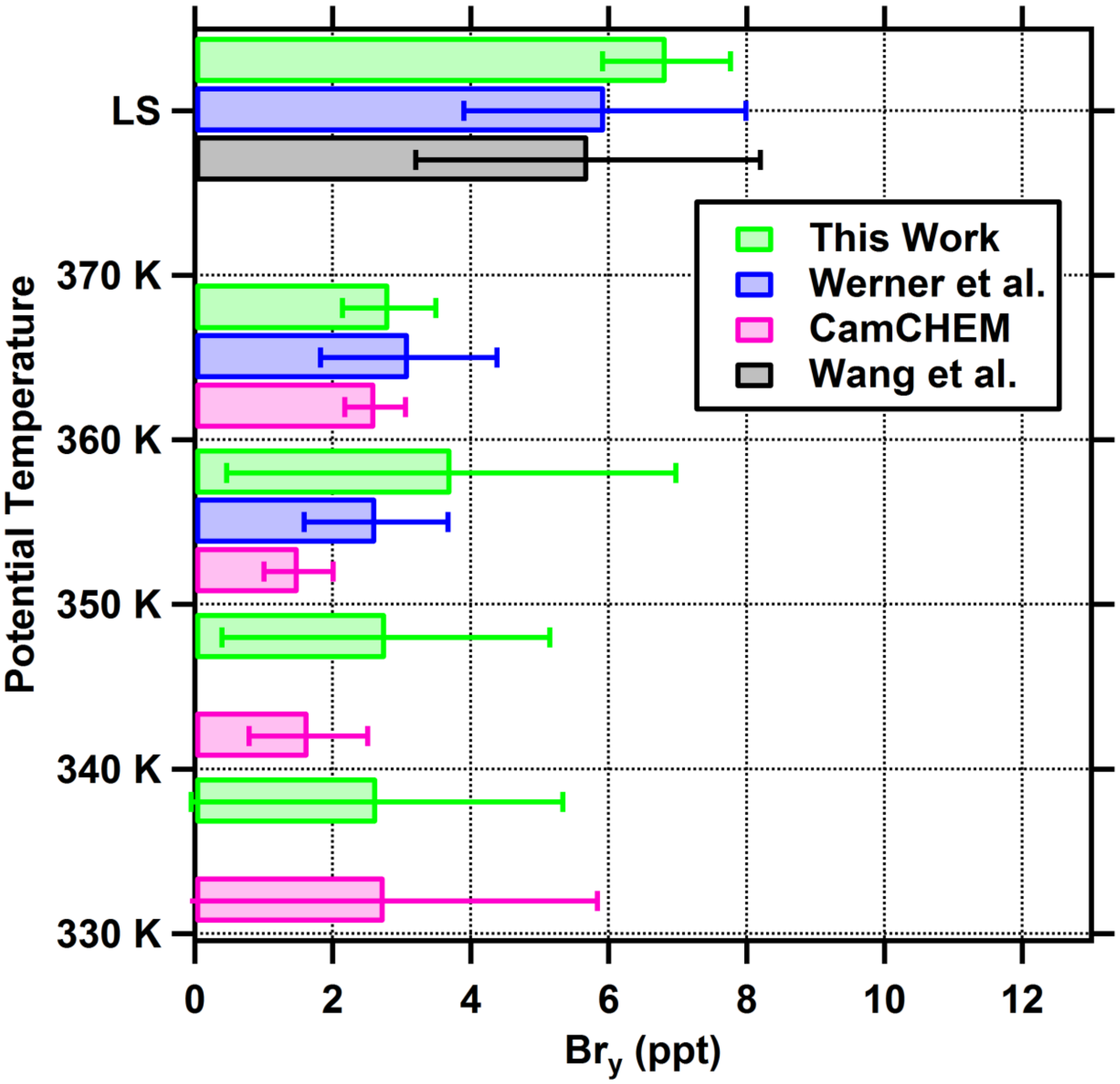

Figure 9: Br_y in the UTLS inferred from BrO observations, and comparison with CAM-chem. Measurements probed BrO over the Southern Hemisphere Eastern Pacific ocean during TORERO (Wang et al., 2015); the Western and Eastern Pacific ocean during ATTREX (Werner et al., 2017), and over the Northern Hemisphere Western Pacific ocean during CONTRAST (this work). CAM-chem results are from this work. For tropospheric air data are presented in 10 K potential temperature (θ) bins. All stratospheric air is pooled (it was sampled at different θ, but is of comparable age; termed old in Werner et al.). Bars indicate the mean Br_y in each bin, and error bars indicate the variances. For this work cases 0-2 are pooled to calculate the means and variances.